PROFESSOR CORA MACALISTER (Orcid ID : 0000-0003-1470-0596)

Article type : Original Article

Exocyst mutants suppress pollen tube growth and cell wall structural defects of *hydroxyproline O-arabinosyltransferase* mutants

Steven Beuder[1], Alexandria Dorchak[1], Ashwini Bhide[1], Svenning Rune Moeller[2], Bent L. Petersen[2] and Cora A. MacAlister[1,*]

1. University of Michigan, Department of Molecular, Cellular and Developmental Biology
2. University of Copenhagen, Faculty of Science, Department of Plant and Environmental Sciences
* corresponding author, macalist@umich.edu

Running Head

Exocyst mutants suppress *hpat* cell wall defects

Keywords

Secretion, pollen tube, cell wall, glycoprotein, suppression, growth, exocytosis, tip growth, exocyst, Arabidopsis thaliana

Summary

HYDROXYPROLINE O-ARABINOSYLTRANSFERASEs (HPATs) initiate a post-translational protein modification (Hyp-Ara) found abundantly on cell wall structural proteins. In *Arabidopsis thaliana HPAT1* and *HPAT3* are redundantly required for full

pollen fertility. In addition to the lack of Hyp-Ara in *hpat1/3* pollen tubes, we also found broadly disrupted cell wall polymer distributions, particularly the conversion of the tip cell wall to a more shaft-like state. Mutant pollen tubes were slow growing and prone to rupture and morphological irregularities. In a forward mutagenesis screen for suppressors of the *hpat1/3* low seed set phenotype, we identified a missense mutation in *exo70a2*, a predicted member of the vesicle-tethering exocyst complex. Suppressed pollen had increased fertility, fewer morphological defects and partially rescued cell wall organization. A transcriptional null allele of *exo70a2* also suppressed the *hpat1/3* fertility phenotype as did mutants of core exocyst complex member *sec15a*, indicating that reduced exocyst function bypassed the PT requirement for Hyp-Ara. In a wild-type background, *exo70a2* reduced male transmission efficiency, lowered pollen germination frequency and slowed pollen tube elongation. EXO70A2 also localized to the PT tip plasma membrane, consistent with a role in exocyst-mediated secretion. To monitor trafficking of Hyp-Ara modified proteins, we generated an HPAT-targeted fluorescent secretion reporter. Reporter secretion was partially dependent on *EXO70A2* and was significantly increased in *hpat1/3* PTs compared to wild type, but reduced in the suppressed *exo70a2 hpat1/3* tubes.

Introduction

For plant cells to grow, the cell wall must be sufficiently extensible to accommodate cell expansion while maintaining enough strength to prevent cell rupture from the high turgor pressure of the cytoplasm. This balance is especially critical to tip growing cell types, like pollen tubes (PTs) and root hairs, where expansion happens at a single growing point. Due to their inherent growth polarity, tip-growing cells may be divided into two general cell wall domains, an extensible tip and a rigid shaft. Cell wall properties depend on its polymer composition and the tip and shaft region differ in functionally significant ways (Rounds et al., 2011; Chebli et al., 2012; Dardelle et al., 2010; Bosch and Hepler, 2005). PTs are generally rich in pectic polysaccharides which are initially secreted in a methyl-esterified form. The methyl-esterified pectins are de-esterified in the wall by pectin methylesterases (PMEs), after which they are able to form a gel through divalent ion cross linking, contributing to cell wall rigidity (Bosch and

Hepler, 2005; Wolf, Mouille and Pelloux, 2009). In PTs, the shaft is further reinforced by the deposition of callose (1,3-β-D-glucan) (Schlüpmann et al., 1994; Van der Woude et al., 1971). In contrast to other plant cell types, PTs contain relatively little cellulose (1,4-β-D-glucan). While cellulose and callose are synthesized at the plasma membrane, other wall polymers are synthesized by ER and Golgi-resident enzymes and must be delivered, along with other secretory cargos, by secretory vesicles, though much is unknown about the process (Cosgrove, 2005; Sinclair et al., 2018).

To support the rapid growth of PTs, secretion must also be very rapid in these cells (Campanoni and Blatt, 2007). Cell expansion and cell wall accumulation are temporally related with secretion leading to thickening of the wall followed by an increase in growth rate during oscillatory PT growth (McKenna et al., 2009). The vesicle dynamics at the tip of the PT are complex and include a mix of exocytic vesicle movement, plasma membrane fusion and endocytic recycling of excess membrane (Bove et al., 2008). Multiple components of the PT secretory pathway have been described including several members of the vesicle tethering exocyst protein complex. The exocyst is an octomeric complex composed of one of each of its subunits (SEC3, SEC5 SEC6, SEC8, SEC10, SEC15, EXO70 and EXO84). The exocyst is well conserved across Eukaryota (Mei and Guo, 2018) and in plants, exocyst complex members have been implicated in several important biological processes including casparian strip formation (Kalmbach et al., 2017), compatible pollen reception by the stigma (Samuel et al., 2009, Safavian et al., 2015), tracheary element development (Li et al., 2013), polar organ growth, root hair elongation (Synek et al., 2006), root growth (Cole, McInally and Fowler, 2014) and pollen germination and tube elongation (Cole, et al., 2005; Hála et al., 2008; Li et al., 2017 and Bloch et al., 2016). However, the rules by which various secretory cargo are packaged and trafficked and how these cargoes become incorporated into a functional wall upon secretion remains poorly understood. The PT is an excellent system for studying these processes given its rapid growth, heavy dependence on secretion and the importance of maintaining proper cell wall organization in these cells.

We have previously shown that successful PT elongation and fertilization requires protein glycosylation, specifically of the hydroxyproline *O*-arabinosylation (Hyp-

Ara) type (MacAlister et al., 2016). O-linked protein glycosylation, like Hyp-Ara, begins in the endoplasmic reticulum with the conversion of peptidyl proline to Hyp by prolyl-4 hydroxylases (Adams and Frank, 1980). In plants, Hyp can be modified by O-linked glycosylation in the form of Hyp-Ara or Hyp O-(arabino)galactosylation (Showalter and Basu, 2016; Tan et al., 2010). Which type of modification a given Hyp receives depends on the protein context; contiguous and non-contiguous Hyps are arabinosylated while clustered but discontinuous Hyp, like those occurring in the arabinogalactan proteins are galactosylated (Kieliszewski and Shpak, 2001, Ohyama et al., 2009). For Hyp-Ara, arabinose sugars are sequentially added until a linear chain of up to 4-5 sugars is formed (Lamport and Miller, 1971). The first, (β1,4-linked) arabinofuranose is added by the Golgi-localized HYDROXYPROLINE O-ARABINOSYLTRANSFERASE 1-3 (HPAT1-3) enzymes which are classified as glycosyltransferase family GT95 members (Ogawa-Ohnishi et al., 2013). The single arabinose (Hyp-Ara_1) may then be extended by the GT77 family members REDUCED RESIDUAL ARABINOSE 1-3 (RRA1-3) and XYLOGLUCANASE113 (XEG113) which add a second (β-1,2-linked) and a third (β-1,2-linked) arabinofuranose, respectively (Egelund *et al.*, 2007; Gille *et al.*, 2009; Velasquez *et al.*, 2011). The fourth (α-1,3-linked) arabinofuranose is added by the GT47-classified EXTENSIN ARABINOSE DEFICIENT TRANSFERASE (ExAD) (Moller et al., 2017). An enzyme activity for addition of the rare fifth arabinose has not been assigned. In the absence of HPAT activity Hyp-oligoarabinosides are not produced (MacAlister et al., 2016). In Arabidopsis, mutants of the three-member *HPAT* gene family have reported pleiotropic effects including reduced hypocotyl length, reduced cell wall thickness, accelerated senescence in *hpat1 hpat2* double mutants, and disrupted root hair elongation (Ogawa-Ohnishi et al., 2013; Velasquez et al., 2015). *HPAT1* and *HPAT3* are redundantly required for full male fertility; *hpat1 hpat2 hpat3* triple mutants and *hpat1 hapt3* double mutants display low male fertility and PT growth defects leading to reduced male transmission and low seed set (MacAlister et al., 2016).

The largest known group of HPAT-target proteins are members of the EXTENSIN (EXT) family of repetitive cell wall structural glycoproteins (Showalter et al., 2010; Brownleader and Dey, 1993; Lamport and Miller, 1971; Lamport, 1967). Following heavy Hyp-Ara modification, EXTs are secreted into the apoplast where they assemble

into an insoluble covalent network by peroxidase-mediated cross-linking of tyrosine residues (Held et al., 2004; Everdeen et al., 1988). The glycosylation of the EXTs contributes to their rod-like, extended poly-Pro-II left-handed helical conformation and increases tyrosine cross-linking *in vitro* (van Holst and Varner, 1984; Stafstrom and Staehelin, 1986a; Stafstrom and Staehelin, 1986b; Chen et al., 2015). This EXT network is hypothesized to serve as scaffold for further cell wall assembly, specifically through acid-base and/or covalent interactions with pectins (Cannon et al., 2008; Qi et al., 1995). Proteins with EXT-like regions fused to other domains are also predicted to carry Hyp-Ara modifications. These “EXT-chimeras” have many proposed functions, with the EXT-like region generally proposed to act in cell wall binding or sensing. EXT-chimeras include the leucine-rich repeat extensin (LRX) proteins, the proline-rich extensin-like receptor kinase (PERK) proteins and the class I formin homology (FH) proteins (Showalter et al., 2010; Borassi et al., 2016).

With the aim of understanding the requirement for Hyp-Ara in PT growth, we carried out a genetic suppressor screen to identify additional factors in the HPAT pollen fertility pathway. Here we report the cloning and characterization of two such suppressor mutants, both of which encode members of the exocyst complex, pointing to an important link between regulation of secretion, protein glycosylation and cell wall structure in the PT.

Results:

To identify mutations suppressing the pollen fertility defect of *hpat1 hpat3* double mutants (*hpat1/3* for brevity) we mutagenized ~2,000 *hpat1/3* seeds by treatment with 0.2% ethyl methanesulfonate. Self-fertilized progeny were screened for increased silique length and seed set (see also Material and Methods section). The identified suppressor mutants, named *fertility restored in hpat1/3* (*frh*), were confirmed to be homozygous for the original *hpat1* and *hpat3* insertion mutations and to display consistently increased fertility between generations and following backcrosses with the parental strain.

frh1 *improves the fertility of* hpat1 hpat3 *pollen*

In contrast to the *hpat1/3* genetic background, suppressed *frh1 hpat1/3* plants showed increased silique length and higher seed set, but appeared otherwise morphologically normal (Fig. 1). To confirm that *frh1* suppression was the result of improved pollen fertility we analyzed seed set following reciprocal crosses between the suppressed line and *hpat1/3*. The *hpat1/3* fertility defect is limited to the pollen; seed set can be fully rescued by pollination with wild-type (WT) pollen (MacAlister et al., 2016). Similarly, seed set was high when *frh1 hpat1/3* was used as the pollen parent, but not when it was used as the seed parent with *hpat1/3* pollen, demonstrating that suppression in *frh1* was due to increased pollen fertility (Fig. 1B). This enhanced pollen fertility coupled with the Arabidopsis habit of producing excess pollen relative to ovule number, impacted the genetic behavior *frh1 hpat1/3* and its pattern of inheritance. Seed set was significantly increased in both homozygous and heterozygous (i.e. backcross F1) *frh1 hpat1/3* plants (Fig. 1B). In the *frh1/+ hpat1/3*, the increased fitness of pollen carrying the *frh1* mutation also drove high *frh1* male transmission and reduced the number of non-suppressed progeny recovered. In a backcross F2 population, only 9% of plants displayed low, *hpat1/3*-like fertility, a significant deviation from the 25% expected in the absence of a transmission bias (N=123, χ^2 P-value = 1.55×10^{-5}).

Given that *frh1* improved *hpat1/3* pollen fertility *in vivo*, we next analyzed the phenotype of *frh1 hpat1/3* PTs directly. When grown on *in vitro* pollen germination media *hpat1/3* PTs displayed a number of defects including reduced PT length, the initiation of secondary tips (i.e. “branched” PTs), high frequencies of PT rupture and modestly increased PT width. We found *frh1* partially suppressed all of these defects (Fig. 1D-E and Fig. S1). Interestingly, we also found that *frh1 hpat1/3* pollen germinated at a lower frequency than either WT or *hpat1/3* pollen. The apparent reduction in germination in *hpat1/3* is at least partially a result of their poor PT growth. *hpat1/3* PTs often rupture and can do so before a tube becomes sufficiently apparent to consider a pollen grain germinated. However, this was not true for *frh1 hpat1/3* pollen grains which had reduced frequency of PT rupture, but further reduced germination frequency. In a comparison of sustained PT growth rates for each genotype, we found an overall reduction in *hpat1/3* PTs which was suppressed by *frh1* (Fig. S1I). Though the *frh1*

hpat1/3 growth rate was even higher than the WT rate, this did not translate into an increase in the overall length of PTs after 5 hours of growth (Fig. 1D). We also noted that *hpat1/3* PTs would often arrest growth for extended periods of time before ultimately rupturing. The average duration of this pre-rupture pausing was 24.5 minutes and ranged from less than five minutes to greater than 100 minutes (N=11).

frh1 does not restore Hyp-Ara, but partially rescues cell wall organization

The most direct mechanism for suppressing the *hpat1/3* phenotype would be restoration of the Hyp-Ara protein modification itself. In order to assess the Hyp-Ara status of *frh1*, we sought an antibody capable of specifically recognizing this modification. The Extensin (EXT) family of cell wall structural proteins are known to be heavily Hyp-Ara modified and several monoclonal antibodies have been previously raised against purified EXTs. We tested three of these for Hyp-Ara specificity (JIM11, JIM19 and JIM20; Smallwood et al., 1994; Smallwood et al., 1995). We found JIM20 recognized protein samples from WT seedlings, but not *hpat* triple mutant seedlings, which we have previously shown to lack detectable Hyp-Ara (Fig. S2A-B; MacAlister et al., 2015). Furthermore, JIM20 did not recognize protein from mutants of the arabinosyltransferases adding the second and third 1→2 linked β-Arabinofuranoses (the *rra2 rra3* double mutants and the *xeg113-3* mutant; Egelund et al., 2007; Gille et al., 2009). JIM20 did however recognize protein from *exad1-1* plants, therefore, the fourth, 1→3 linked α–arabinofuranose added by ExAD is not required for JIM20 recognition (Moller et al., 2017). We immuno-labeled pollen grains and PTs with JIM20 to determine the localization of Hyp-Ara in these cells. We found robust staining of the WT pollen grain and tube cell wall (Fig. 2A, Fig. S2C). In *hpat1/3* pollen, we detected no JIM20 signal, as in WT secondary antibody alone controls (Fig. S2D-E). As in *hpat1/3*, no Hyp-Ara was detected in *frh1 hpat1/3* tubes (Fig. S2F). Therefore, *frh1* did not suppress the *hpat1/3* phenotype by directly restoring Hyp-Ara, but through another mechanism.

The *hpat1/3* pollen phenotypes are consistent with defective cell wall integrity. In order to gain insight in the molecular basis for these defects and *frh1*'s suppression of them, we compared the organization of key PT cell wall polymers. Given the importance of pectin for PT growth and the proposed function of EXTs in pectin organization we

hypothesized that compromised EXT Hyp-Ara may alter pectin distribution in the cell wall. We used the monoclonal antibodies LM19 and LM20 (Verhertbruggen et al., 2009) to assess the distribution and abundance of demethyl-esterified homogalacturonan (dme-HG) and methyl-esterified HG (me-HG), respectively, in WT, *hpat1/3* and *frh1 hpat1/3* PTs. A key functional difference between these two forms of pectin is their ability to form calcium salt bridges. dme-HG is able to form a cross-linked structure while the methyl-ester groups present on the me-HG prevent this (Micheli, 2001). In WT PTs, the me-HG recognized by LM20 was enriched at the PT tip while the calcium cross-linkable dme-HG recognized by LM19 was excluded from the tip and enriched in the shaft, consistent with previous reports (Fig. 2C-D; Rounds et al., 2011; Chebli et al., 2012; Dardelle et al., 2010; Bosch and Hepler, 2005). This pattern was disrupted in *hpat1/3* PTs. The LM20 epitope (me-HG) signal enrichment at the tip region was weaker in *hpat1/3*. Moreover, the overall level of LM19 epitope (cross-linkable dme-HG) was increased in the shaft region and enriched, rather than excluded from the tip (Fig. 2C-D). However, *frh1 hpat1/3* PTs had intermediate levels of dme-HG (LM19) signal, and reduced me-HG (LM20) at the tip relative to the shaft, though the pattern was not restored to that of WT. Increased cell wall rigidity at the PT tip in *hpat1/3* due to accumulation of dme-HG in this region is consistent with the poor expansion ability of this genotype. The reduced accumulation of this polymer in *frh1* is also consistent with its improved growth and the suppressed phenotype. Interestingly, in *frh1 hpat1/3* PTs, the tip enrichment of me-HG (LM20 signal) was almost completely missing and the expression was generally flat across the length of the PT (Fig. 2C).

The PT shaft is also reinforced with callose (Schlüpmann et al., 1994; Van der Woude et al., 1971). We stained PTs with aniline blue fluorochrome (ABF) to compare callose distribution between genotypes. As expected, in WT PTs we found high levels of ABF binding along the shaft and low signal at the tip. Again, consistent with the poor expansion ability of *hpat1/3* pollen, we found high levels of ABF signal at the PT tip. This enrichment was abrogated in *frh1 hpat1/3* tubes, though not restored to WT levels, again, consistent with the improved growth of suppressed PTs (Fig. 2B).

frh1* suppression is caused by a mutation in *exo70a2

To identify the mutation conferring increased seed set and improved PT growth in *frh1* plants, we used a high-throughput sequencing strategy (Beuder and MacAlister, 2020). *frh1* was backcrossed to the parental strain for four generations and allowed to self-fertilize forming the BC4 F2 generation. To identify homozygous *frh1* individuals for sequencing, the BC4 F2 plants were used as females in test crosses with *hpat1/3* pollen. Homozygous *frh1* plants produce only suppressed F1 progeny while heterozygous females produce a 1:1 ratio of suppressed and non-suppressed progeny. A minimum of 11 test cross progeny per parent were scored for 25 BC4 F2 individuals. Twelve were found to be homozygous (100% suppressed progeny, N=149 total), while the remaining 13 were heterozygous (49.4% suppressed progeny, N=170 total). We extracted DNA from three groups of plants: the self-fertilized progeny of the confirmed homozygous *frh1* plants (the *frh1/frh1* pool), the non-suppressed progeny segregating from the heterozygous plant test crosses (the *FRH1/FRH1* pool) and the *hpat1/3* genetic background.

Following paired-end 150 bp DNA sequencing, quality control and read mapping, we identified sequence variants from all three DNA samples relative to the Columbia reference genome (Table S1). From the variants identified in the *frh1/frh1* data, we removed all variants shared with the background strain (*hpat1/3*) or the *FRH1/FRH1* pool, leaving 18,287 unique *frh1* variants. We filtered this set for single nucleotide polymorphisms, as expected for an EMS-induced mutation, supported by a minimum of four reads leaving 16,001 variants. After filtering for a minimum variant sequence read frequency of 80%, we were left with 48 variants, eight of which were predicted missense mutations. Thirty of these variants were clustered within a 5.7 Mbp region on chromosome 5, presumably containing the causative mutation and those linked to it (Table S2). Near the middle of this region, we identified a missense mutation converting glycine 319 to a glutamic acid in EXO70A2, a predicted subunit of the vesicle-tethering exocyst complex. The altered amino acid position (Glycine 319) is conserved in eight of the 23 Arabidopsis EXO70s including the A, E, F and G subfamilies and is directly C-terminal to a phenylalanine that is conserved in all Arabidopsis EXO70s (Fig. S3).

We tested for co-segregation between the *exo70a2*^{G319E} variant (hereafter *exo70a2-2*) and the suppressive phenotype in an *frh1* BC5 F2 population using a PCR-based genotyping assay. As expected for the causative mutation, we found a significant bias against recovery of homozygous wild-type plants and perfect concordance between *exo70a2-2* genotype and suppressive phenotype, including intermediate seed set values for heterozygous plants (Fig. S4). To confirm that the *exo70a2* mutation is the cause of the *frh1* suppression, we expressed the wild-type genomic *EXO70A2* sequence from a transgene in the *frh1 hpat1/3* background. Transgenic *frh1* "rescue" would be a return to the low fertility of the *hpat1/3* parental strain. We cloned a 3,971 bp region of the EXO70A2 locus including the native promoter, full coding region and ~450 bp of 3' sequence and recombined this fragment into a plant expression vector containing a seed-expressed fluorescent transformation marker (Shimada, Shimada and Hara-Nishimura, 2010). We compared the transgene transmission efficiency in three independent single-loci insertion hemizygous lines and found a significant and robust male-specific transmission defect for the *EXO70A2* transgene for all lines (Fig. S5). The same plasmid backbone carrying a strong pollen-specific promoter (Lat52) driving expression of the florescent protein, mNeonGreen, had no effect on male or female transmission (Fig. S5B; Bate and Twell, 1998; Shaner et al., 2013). Furthermore, in *exo70a2-2 hpat1/3* lines homozygous for the transgene, seed set was reduced to the level of the *hpat1/3* background while non-transgenic sibling plants had *frh1*-like high seed sets (Fig. S5C). Thus confirming that the *exo70a2-2* mutation confers the increased fertility observed in *frh1 hpat1/3* plants.

EXO70A2 *is required for efficient pollen germination and pollen tube growth*

Given the effect of *exo70a2-2* on *hpat1/3* pollen fertility, we next determined the phenotypic consequence of this mutation in an otherwise WT background. From a Col outcross population, we isolated *exo70a2-2* homozygous mutants which were wild-type for *HPAT1* and *HPAT3*. We observed no statistically significant change in seed set between Columbia and *exo70a2-2* (Fig. 3C). However, using a more sensitive competitive fertilization assay, we found significantly reduced male transmission of the *exo70a2-2* allele vs. the WT allele (16.7% transmission efficiency, N=84; χ^2 P-

value=5.89x10^{-11}). Therefore, in an otherwise WT background, *exo70a2-2* reduced pollen fitness.

Since we had observed partial rescue of cell wall organization in suppressed PTs (Fig. 2), we compared the PT cell wall organization between WT and *exo70a2-2*. We again used LM19 and LM20 to compare the distribution of dme-HG and me-HG, respectively along with ABF staining to compare callose accumulation. In all three cases, the overall pattern of signal was similar between WT and *exo70a2-2* tubes (Fig. S6). The only difference we observed was an overall reduction of signal intensity for LM19 (dme-HG) in *exo70a2-2*, though the pattern of low signal at the tip and increasing signal in the shaft was the same for both genotypes. We next used the JIM20 antibody to compare distribution of Hyp-Ara. Similar to our observations for LM19 staining, the overall intensity of JIM20 signal was reduced in *exo70a2-2* PTs, though the pattern was generally flat across the PT length in both genotypes. Therefore, while *exo70a2-2* partially restores PT cell wall organization in the *hpat1/3* background, it did not alter cell wall polarity in the wild-type background.

Our transgenic rescue data (Fig. S5) suggests that the G319E allele is likely a loss or reduction of function allele and the only previously published allele (*exo70a2-D*) is a promoter-region insertion with increased transcript expression with no reported pollen fertility phenotypes (Synek et al., 2017). To gain further insight into the function of this gene, we identified an additional allele with an insertion in the fifth intron of *EXO70A2* among the available insertion mutant collections. Based on RT-PCR analysis of flower cDNA, we found that this insertion mutant (*exo70a2-3*) was a transcriptional null allele (Fig. 3B). Seed set was modestly reduced in homozygous *exo70a2-3* plants compared to the WT background (Fig. 3C-D) and the male transmission efficiency of *exo70a2-3* was also reduced to about half of the *exo70a2-2* value (8.3% transmission efficiency, N=130, χ^2 P-value=5.03x10^{-22}). We next tested *exo70a2-3* for suppression of the *hpat1/3* low-fertility phenotype. Self-fertilized progeny of *exo70a2-3/+ hpat1/3* plants displayed a significant bias towards inheritance of the *exo70a2-3* mutant allele, consistent with a suppressive effect conferring improved transmission of the triple mutant pollen (13% WT, 49% heterozygous, 37% homozygous mutant, N=67 total, χ^2 P-value=7.06x10^{-9}). Seed set in *hpat1/3 exo70a2-3* triple mutants was also significantly

increased compared to the *hpat1/3* background, though the *exo70a2-3* allele did not increase seed set to the same degree as the *exo70a2-2* allele (Fig. 3C).

Since *exo70a2* mutants exhibit reduced male fitness in the wild-type background, we analyzed their pollen phenotypes directly. When grown *in vitro* we observed a moderate and strong reduction in pollen germination frequency for *exo70a2-2* and *exo70a2-3*, respectively (Fig. 3E-G). The non-germinated pollen grains appeared morphologically normal and all pollen appeared similarly viable based on Alexander staining (Fig. 3H-J; Peterson, Slovin and Chen, 2010). We hypothesize the observed germination defect was due to failure to target secretory vesicles to the germination site, similar to the pollen germination defect described for other exocyst mutants including *sec3a,* sec6, *sec8, sec15a* and *sec5* (Li et al., 2017; Bloch et al., 2016; Cole et al., 2005; Hála et al., 2008). We examined germination plaque formation using Ruthenium red which stains pectin accumulation (Li et al., 2017). Though WT pollen accumulated pectin at the germination site as expected, most *exo70a2-3* pollen did not, consistent with the low germination frequency in this line (Fig. 3K-L). We further noted that the mutant pollen which successfully germinated produced shorter PTs than the wild type after five hours of growth (Fig. 3M), though they were otherwise morphologically normal (Fig. 3O-P). To determine if this was due to slower rates of PT growth or an indirect effect of delayed germination, we measured the sustained PT growth rate. Following successful germination, *exo70a2-3* PTs elongated at about half the rate observed in WT though the rate of *exo70a2-2* PT growth was not significantly different from that of the WT (Fig. 3N). Therefore, *exo70a2* mutants have both impaired pollen germination and tube elongation, phenotypes consistent with a secretion defect, with the *exo70a2-3* null allele being more severely impaired than the missense allele *exo70a2-2*.

EXO70A2 *localizes to the tip of growing pollen tubes*

Available microarray, mRNA sequencing and proteomic data indicates that *EXO70A2* is most strongly, if not exclusively expressed in pollen and PTs (Synek et al., 2017; Hruz et al., 2008; Klepikova et al., 2016; Grobei et al., 2009). To validate this expression data and determine the sub-cellular localization of EXO70A2, we generated a C-terminal mNeonGreen fusion protein including the native promoter region and full

genomic sequence (EXO70A2-mNG). In stably transformed wild-type plants, we observed reporter expression in *in vitro* grown PTs, with no detectable expression in other tissues, in agreement with the reported expression data. To determine if the fusion protein was functional, we transformed homozygous *exo70a2-3* plants with this construct. In contrast to the low germination frequency of *exo70a2-3* pollen, pollen from three independent T1 plants had a significantly higher proportion of germinated pollen grains after two hours and the vast majority of T1 PTs were positive for mNeonGreen fluorescence, demonstrating that pollen carrying the reporter construct was able to germinate and form elongating PTs while the non-transgenic mutant pollen largely failed to do so (Fig. S7). A similar experiment using the EXO70A2^{G319E} point mutant fused to mNeonGreen resulted in much weaker rescue of pollen germination frequency, suggesting that this mutant is a hypomorph with reduced activity relative to the wild-type sequence (Fig. S7B). In addition to the weaker rescue by the mutant protein, the resulting PTs had noticeably weaker fluorescence than the corresponding wild-type EXO70A2-mNG expression lines, suggesting the mutant protein may be less stable *in vivo*, potentially accounting for its lower activity.

In budding yeast, EXO70p localizes to the target membrane, along with SEC3p, through phospholipid interactions and recruits the remaining, vesicle-associated complex members to the site of tethering (He et al., 2007; Liu et al., 2007). Given the importance of proper vesicle targeting during tip growth, we examined the localization of the EXO70A2:mNG fusion protein in PTs and observed signal at the tip plasma membrane (Fig. 4). This localization pattern was similar to the immunolocalization pattern reported by Hála et al., (2008) in tobacco PTs using an antibody raised against the highly similar EXO70A1. Furthermore, a C-terminal YFP fusion to the tobacco EXO70A2 homologue (NtEXO70A2) was reported to localize to the PT tip, but only occasionally to show PM localization (Sekeres et al., 2017).

exo70a2 mutants reduce Hyp-Ara modified protein secretion at the pollen tube tip

EXO70A2's localization to the PT tip (Fig. 4), combined with the reduced pollen germination and slower PT growth of *exo70a2-3* mutants (Fig. 3) suggested that EXO70A2 is a positive regulator of PT tip growth and likely acting as a canonical

exocyst complex member. Therefore, we hypothesized that the suppression of *hpat1/3* by *exo70a2* mutants was due to reduced rates of secretion of one or more key exocyst cargo(s). Hyp-Ara modified proteins themselves are a strong candidate for exocyst-mediated secretion. To develop a secretion reporter to allow us to follow Hyp-Ara modified proteins, we used a portion of a directly validated HPAT substrate, EXT3 (Ogawa-Ohnishi et al., 2013), specifically an arabinosylation motif (SPPPP) and adjacent sequence (KSPPPPVKHLY) inserted into an exposed loop of GFP (Fig. 5A). Insertion into the GFP sequence has been shown to stabilize glycoprotein fusions which are otherwise often subject to terminal tag cleavage and degradation (Yang, Bennett et al., 2012). We used the EXT3 signal peptide sequence to drive the protein into the secretory pathway and expressed the resulting fusion, GF(EXT3)P, under the Lat52 promoter for pollen expression (Bate and Twell, 1998). We stably transformed this construct into *hpat1/3* plants. To limit potential confounding effects due to expression level variation between independent transgenic lines, we crossed a single, robustly expressing *hpat1/3* GF(EXT3)P line to Col, *exo70a2-2*, *exo70a2-3* and *hpat1/3 exo70a2-2* and isolated the desired genotypes from the resulting F2 populations. As a control, we also transformed a GFP construct with no signal peptide (Lat52::GFP) into Col.

We were able to detect GF(EXT3)P from PT protein samples with an anti-GFP polyclonal antibody at the expected molecular mass of the fusion, ~34 KDa (Fig. 5B). To determine if the fusion protein was arabinosylated, we probed with the JIM20 Hyp-Ara antibody. No native arabinosylated proteins of the GF(EXT3)P mass were observed in un-transformed Col PTs, but we detected JIM20 signal at the observed reporter mass in the GF(EXT3)P transgenic Col line (Fig. 5B). No JIM20 signal was detected from *hpat1/3* or *exo70a2-2 hpat1/3* transgenic samples, consistent with the absence of Hyp-Ara in these genotypes.

In *in vitro* grown GF(EXT3)P-expressing PTs, we observed robust intracellular fluorescence, likely due to the presence of the reporter in the secretory pathway (ER, Golgi and secretory vesicles). To determine if the protein was secreted, we plasmolyzed PTs by transfer to high sucrose media. In PTs, plasmolysis occurs preferentially at the tip region, separating the plasma membrane from the cell wall (Hill et al., 2012). We

observed fluorescence signal remaining at the vacated PT tip, suggesting that the protein was secreted into the cell wall space (Fig. 5C). To quantitatively compare secretion between genotypes, we calculated a “Secretion Index” (SI) as a ratio of fluorescence intensity of the cytoplasm-free tip region to the intracellular signal after subtraction of non-tube background. The Col GF(EXT3)P SI was significantly higher (~3-fold greater) than that of the control GFP construct, demonstrating that the GF(EXT3)P construct was actively secreted (Fig. 5D). This secretion was also partially dependent on *EXO70A2;* the SI was significantly lower in *exo70a2-3* compared to WT PTs, though it was still greater than the SI of the control (Fig. 5E). Interestingly, the SI was increased by ~40% in *hpat1/3* mutants compared to Col, suggesting more rapid secretion of HPAT-target proteins in the absence of the HPATs, despite the lower growth rate of the *hpat1/3* tubes (Fig. S1I). Finally, we found that the Secretion Index was significantly reduced in the suppressed *hpat1/3 exo70a2-2* PTs compared to *hpat1/3*, but was not significantly different from the *exo70a2-2* value. Thus, in addition to the cell wall defects of *hpat1/3* PTs noted above, increased secretion of un-modified HPAT-target proteins may be further confounding the cell wall structure of the mutant PTs.

sec15a mutants also suppress the hpat1/3 fertility phenotype

The above data suggests an important function for *EXO70A2* in the secretion of glycoproteins in PTs. The *exo70a2* mutant phenotypes were also consistent with the defects observed for mutants in other exocyst complex members (Cole, et al., 2005; Hála et al., 2008; Li et al., 2017 and Bloch et al., 2016). If the underlying mechanism of *hpat1/3* suppression by *exo70a2* is a reduction of exocyst-mediated secretion, mutants in other members of the core exocyst should also suppress the *hpat1/3* fertility defects. Fortuitously, in the course of sequencing additional *frh* suppressor lines, we identified a line carrying a mutation in exocyst complex member *SEC15A,* converting serine 213 to phenylalanine (Table S3, Fig. 6A). *SEC15A* is one of two Arabidopsis *SEC15* genes and is required for male transmission, pollen germination and PT growth (Hála et al., 2008). In the BC5 F2 generation of this suppressor family, we found strong bias against recovery of plants homozygous for the wild-type *SEC15A* allele, as expected for an

hpat1/3-suppressing mutation (Fig. 6B-C, χ^2 P-value = $1.57x10^{-5}$). Following pollination of *hpat1/3* pistils by pollen from *sec15a-3/+ hpat1/3* plants, 90% of the progeny inherited the *sec15a-3* allele (61 heterozygous vs. 7 WT progeny, χ^2 P-value = $5.8x10^{-11}$), confirming increased male transmission of the *sec15a*^{S213F} mutation (hereafter *sec15a-3*) in the *hpat1/3* background. We also found perfect co-segregation between *sec15a-3* and the suppressive phenotype including intermediate seed set values for heterozygous individuals (Fig. 6D). Like *exo70a2-2*, the *sec15a-3* mutant also increased PT lengths *in vitro* in the *hpat1/3* background (Fig. 6E). After outcrossing our suppressor allele to the wild-type Columbia background to remove the *hpat1* and *hpat3* mutations, *sec15a-3* mutants did not display significantly different seed set compared to WT, similar to our observations for *exo70a2-2* (Fig. 6D and Fig. 3C). However, the transmission efficiency of the mutant allele was reduced in the WT background (TE=60.6%, N=249, χ^2 P-value = $1.1x10^{-4}$), indicating a modest fertility cost to pollen carrying the mutant allele.

Given that loss of function *exo70a2* mutants were able to suppress the *hpat1/3* phenotype, we reasoned that the suppression by *sec15a-3* was also due to a loss of function of this core exocyst complex member. Therefore, we next crossed *hpat1/3* to a previously published transcription null T-DNA insertion allele of *sec15a* (*sec15a-2*, SALK_067498; Hála et al., 2008). In plants homozygous for the *hpat1* and *hpat3* mutations, the presence of a *sec15a-2* allele increased seed set with homozygous *sec15a-2* plants being more strongly impacted (Fig. 6D), thus confirming that loss of function of *sec15a* can suppress the *hpat1/3* phenotype. The recovery of homozygous *sec15a-2* plants in the *hpat1/3* background was somewhat surprising since this allele is essential for male transmission in the WT background (Hála et al., 2008).

If *exo70a2* and *sec15a* both suppress the *hpat1/3* fertility defect through disruption of the same protein complex, plants carrying both mutations should exhibit no further suppression relative to the single suppressor mutants. We crossed the two suppressor families to establish the genetic relationship between them. In the double suppressor genotype (i.e. *hpat1/3 exo70a2-2 sec15a-3* quadruple mutants) we observed the same level of seed set as sibling *hpat1/3 exo70a2-2* plants and a minor, but statistically significant (T-test P-value 0.03) increase compared to the *hpat1/3*

sec15a-3 siblings (Fig. 6G), consistent with the hypothesis that both suppress through disruption of the core exocyst complex.

Discussion

PTs grow by the targeted secretion of new cell wall material to their tip. We have previously shown that the plant-specific protein modification hydroxyproline O-arabinosylation (Hyp-Ara) is required for proper PT growth and full male fertility (MacAlister et al., 2016). Here, we report major changes in the organization of the PT cell wall in *hpat1/3* mutants, specifically a loss of PT cell wall polarity and the conversion of the normally extensible cell wall structure at the PT tip into a more shaft-like state (Fig. 2). While immunolocalization studies of cell wall epitopes must be interpreted with caution due to potential epitope masking by interaction between polymers, our results demonstrate a change in cell wall organization in the *hpat1/3* PTs. Once the tip wall is disrupted as in the *hpat1/3* tubes, one would expect cell expansion to be compromised, leading to growth arrest and/or PT rupture. The “branching” observed for *hpat1/3* PTs may be the result of growth being re-directed to a more viable sub-apical cell wall region (Fig. S1). The EXT family of cell wall structural glycoproteins are heavily Hyp-Ara modified, therefore, the most direct explanation for the disrupted cell wall organization of the *hpat1/3* PTs is that the lack of Hyp-Ara prevents proper EXT function in the cell wall, broadly disrupting cell wall organization. The un-modified EXTs may also be toxic to cell wall structure; their presence as un-arabinosylated proteins causing greater disruption to the wall than their absence would. Loss-of-function mutants of the exocyst components *exo70a2* and *sec15a* suppress the *hpat1/3* pollen fertility phenotype, suggesting that reducing the rate of secretion of one or more key exocyst cargoes allows *hpat1/3* PTs to compensate for their defects. This is apparent as a partial restoration of PT cell wall organization, particularly a reduction of the anomalous accumulation of dme-HG and callose at the PT tip (Fig. 2) and an increased PT growth rate (Fig. S1I).

To determine if HPAT-modified proteins themselves are trafficked through the exocyst, we generated a Hyp-Ara modified secreted reporter (GF(EXT3)P). The secretion index (SI) of GF(EXT3)P was significantly reduced in PTs of the null *exo70a2*-

3 allele compared to WT PTs (Fig. 5), indicating that reporter secretion was, at least partially, *EXO70A2* dependent. However, the *exo70a2-3* GF(EXT3)P SI was still above the SI of the GFP control. Thus, there may be exocyst-independent secretion of GF(EXT3)P, or functional redundancy within the 23 member *EXO70* gene family. Several other *EXO70* genes are expressed in PTs and two (*EXO70C1* and *EXO70C2*) have demonstrated PT functions, though their mutant phenotypes are qualitatively distinct from those of other exocyst complex mutants, suggesting they may be regulators of exocyst function rather than canonical exocyst components (Chong et al., 2009; Li et al., 2010; Synek et al., 2017; Hruz et al., 2008; Klepikova et al., 2016; Grobei et al., 2009). A recent preprint characterizing a CRISPR/Cas9 induced *exo70a2* mutant allele agrees with our findings with respect to the importance of *EXO70A2* for pollen germination and pollen tube elongation, further supporting its central role in PT exocytosis (Markovic et al., 2019). Furthermore, reduced secretion of Hyp-Ara modified proteins in *exo70a2* mutants would also be consistent with the reduced levels of JIM20 staining we observed in *exo70a2-2* PTs (Fig. S6). The reduced SI of the GF(EXT3)P reporter in the *exo70a2* mutant indicates that the protein is being retained cytoplasmically. This retention may be occurring in secretory vesicles, at earlier points in the secretory pathway (e.g. the Golgi apparatus), or in another compartment. Determining the site of retention will require co-localization with sub-cellular markers. We also found that *hpat1/3* PTs had the highest GF(EXT3)P SI of any genotype (Fig. 5). Enhanced secretion of a glycoprotein in the absence of the relevant glycosyltransferases has been previously noted in other systems, though the underlying mechanism is unknown. For example, in budding yeast, mutation of mannosyltransferases required for N-linked hypermannosylation of cell wall glycoproteins resulted in increased secretion of modified heterologous proteins (Tang et al., 2016). Knockdown of Golgi stacking proteins also led to reduced glycosylation and accelerated secretion (Xiang et al., 2012). The underlying cause of increased glycoprotein secretion in *hpat1/3* is unclear. Partial arabinosylation could serve as a Golgi retention signal, preventing premature target protein secretion, and since the *hpat1/3* PTs cannot initiate arabinosylation, such a retention signal would be absent. Alternatively the presence of the HPAT enzymes themselves may be required for target

protein retention. The *hpat1* and *hpat3* alleles are transcriptional nulls (MacAlister et al., 2016), thus any protein/protein interactions they participate in would be disrupted in *hpat1/3* mutants. Alternatively, other compensation pathways may be activated in the hapt1/3 tubes, leading to an indirect increase in secretion. Regardless of the cause of the elevation in *hpat1/3* PTs, the secretion index was significantly reduced in *exo70a2-2 hpat1/3* PTs.

While the GF(EXT3)P secretion reporter showed that the secretion rate was altered for a synthetic HPAT-modified protein, which native protein(s) are important for PT growth is more difficult to determine. The list of candidate proteins for HPAT-modification is long, and includes the 20 classical Arabidopsis EXTs and multiple EXT-chimera families including the LRX, PERK and class I FH proteins (Showalter et al., 2010). Several members of each of these gene families are expressed in pollen. For example, six members of the *PERK* family of 15 genes are highly or exclusively expressed in pollen samples in Arabidopsis (Borassi et al., 2016). The class I Formin Homology genes, *FH3* and *FH5*, are also expressed in pollen and known to be important regulators of PT growth through their regulation of the actin cytoskeleton (Ye et al., 2009; Cheung et al., 2010; Cheung and Wu, 2004). The *LRX* genes include four members (*LRX8-11*) which are expressed specifically in pollen and have been shown to redundantly contribute to pollen fertility. Higher order *lrx* mutants displayed reduced pollen germination, abnormal PT morphology and frequent tube rupture (Fabrice et al., 2018; Sede et al., 2018; Wang et al., 2018). LRX proteins have also been shown to bind to the RALF4/19 peptides and participate in an autocrine signaling loop maintaining PT integrity until reaching the ovule (Mecchia et al., 2017). Furthermore, Fabrice et al. (2018) also demonstrated reduced levels of JIM20 signal in *lrx8/9* and *lrx8/9/11* mutant PTs. This could be interpreted as a direct reduction in Hyp-Ara in these mutants due to reduced LRX protein levels, though an indirect effect involving feed-back with other modified proteins can't be ruled out.

In addition to the EXTs and EXT-chimeras, a second, unrelated group of HPAT-modified proteins is currently known, the small secreted signaling peptides of the CLAVATA3/EMBRYO-SURROUNDING REGION-RELATED (CLE) family. Mutants of HPAT family members from tomato, Medicago truncatula and Lotus japonicus function

in the regulation of shoot meristem size and the determination of nodule number through their effect on CLE peptide arabinosylation (Xu et al., 2015; Schnabel et al., 2011; Kassaw et al., 2017; Yoro et al., 2019; Imin et al., 2018). While the participation of an HPAT-modified CLE peptide in PT growth is an intriguing possibility, no candidates for such a pollen-expressed CLE are forthcoming (Kanaoka and Higashiyama, 2015).

Moreover, while we demonstrated reduced secretion of a Hyp-Ara modified reporter protein in the suppressed PTs (Fig. 5D), this does not preclude the trafficking of other cargoes through the exocyst. Slowing the delivery of cell wall polysaccharides or non-arabinosylated cell wall modifying enzymes may also contribute to *hpat1/3* suppression by exocyst mutants. In the PT, pectins are initially secreted in the methyesterified form and then de-methylesterified in the wall by pectin methyl esterases (PMEs), which are in turn regulated by PME inhibitors (PMEIs; Bosch and Hepler, 2005). Altering the rate of delivery of pectin, PME and/or PMEI proteins could alter the timing of de-methylesterification in the PT wall. There is evidence of exocyst involvement in pectin secretion in the specialized seed coat mucilage cells (Kulich et al., 2010). The exocyst is also involved in the secretion of cellulose synthase complexes (Zhu et al., 2018) and may be trafficking other, similar complexes in the PT, for example, callose synthases.

Evidence is mounting that secretion is likely to be more complex than a simple bulk flow of Golgi material to the plasma membrane. Data from budding yeast has shown distinct post-Golgi secretory vesicles carrying different sets of cargoes marked by the presence of Bgl2p or invertase, with mutations in *exo70* predominantly blocking secretion of Bgl2p-containing vesicles (Harsay and Bretscher, 1995; He et al., 2007b). In plant cells there is also evidence of distinct trafficking pathways for reporter proteins vs. cell wall polysaccharides (Leucci et al., 2007). The trafficking landscape of PTs is likely to be complex and subject to tight regulation.

Materials and Methods

Plant growth conditions and materials

Arabidopsis thaliana plants of the Columbia-0 ecotype were grown under 16-hour light: 8-hour dark cycles in a temperature-controlled growth room maintained at 23˚C. Recovery of *hpat1-2* (Salk_120066) *hpat3-1* (Salk_085603) double mutants has been previously described (MacAlister et al., 2016). *frh* mutants were induced by treatment of *hpat1/3* seeds with 0.2% EMS for 12 hours. Seeds from the mutagenized plants were collected in pools of 5-10 M1 plants and ~96 M2 individuals per pool were screened for increased silique length and higher seed content. *frh* candidates were genotyped for the *hpat1* and *hpa3* mutant alleles to confirm homozygosity and backcrossed to the *hpat1/3* background for four generations. The *exo70a2-3* (WiscDsLoxHs216_02A; Woody et al., 2007) and *sec15a-2* (SALK_067498; Alonso et al., 2003) insertion alleles were obtained from the ABRC. Mutants were genotyped using the primers listed in Table S4. RT-PCR for *exo70a2-3* knockout validation used the *EXO70A2* primers given by Synek et al. (2017) and primers from Table S4. The *rra2* (SAIL_244_A03)*, rra3* (Gabi 223B05), *xeg113-3* (SALK_058092)*,* and *exad1-1* (SAIL_843_G12) insertion alleles were genotyped using the primers listed in Table S4. To clear siliques for seed counts, fully expanded, but unripe siliques were transferred to 70% ethanol for at least two days, after which, the ethanol was replaced with 50% glycerol for several more days.

Whole-genome sequencing

After four generation of backcrossing of the *frh* plants to *hpat1/3*, suppressed F2 plants were crossed as females to *hpat1/3* plants to identify homozygous and heterozygous individuals based on suppression segregation in the cross progeny. Self-fertilized seeds from confirmed homozygous BC4 F2 plants were germinated on MS media plates for DNA extraction as were seeds of the *hpat1 hpat3* background strain. Tissue for the FRH/FRH pool was collected from non-suppressed plants produced by the heterozygous test cross progeny. DNA was extracted from the tissue pools using the Qiagen Plant DNA Mini kit according to the manufacturer's instructions, followed by concentration by ethanol precipitation. Libraries were generated using Illumina TruSeq DNA kits and barcoded for multiplexing by the University of Michigan DNA Sequencing Core. Samples were sequenced on the Illumina HiSeq-4000 platform with paired-end

150 bp cycles. Sequence reads were checked for quality using FastQC then aligned to the TAIR10 genome using Bowtie2, and sequence variants were called using Freebayes. Additional analysis steps were performed with Samtools. We identified all the mutations in each suppressor family and removed mutations that were also present in the *hpat1/3* and/or the FRH/FRH samples. We then filtered the mutations based on allelic frequency ≥ 0.8, mutation type = SNP and read number ≥ 4. We annotated the sequence variants for context and predicted effect using a custom PERL script.

JIM20 dot blot and western blot analysis

Total non-covalently-bound protein was extracted from Col, *hpat1/2/3*, *rra2/3*, *xeg113* and *exad* seedlings grown on MS plates using a procedure modified from Fry (1988). Tissue was ground in liquid nitrogen and resuspended in freshly prepared solution A (100ml acetic acid, 250ml 80% w/w phenol), stirred rapidly in a fume hood at 70°C for 30 minutes, and cooled prior to filtering through GF/C glass fiber paper in a 4.25cm porcelain Buchner funnel (VWR, 470153-508). The residue was rinsed twice with 5ml of solution B (35ml solution A, 5ml H_2O), then 2.5ml of 10% ammonium formate. 255ml acetone was added to the filtrate, and incubated on ice for an hour. The protein precipitate was spun in PYREX™ round-bottom glass centrifuge tubes (Fisher, 05-558-5B) for 5 minutes at 2,500 x g, the supernatant discarded, and the pellet resuspended in 10ml 10% acetone. After a second spin for 5 minutes at 2,500 x g, the protein was resuspended as much as possible in a minimal volume of H_2O (1-5ml) and its concentration determined using a BCA protein assay kit (Pierce, 23225). For dot blots, 5μg of total protein extract was spotted onto 0.2μm nitrocellulose and allowed to dry prior to immuno-processing. For western blots, 15μg of total protein extract was separated by 10% mini-PROTEAN® TGX™ (Bio-Rad, 456-1033) gel electrophoresis and transferred onto a 0.2μm PVDF membrane (Bio-Rad, 170-4156) using the Trans-Blot® Turbo™ transfer system. Dot blots and western blots were then blocked for 1 hour (5% milk, in 1x TBST), probed with 1:10 JIM20 monoclonal rat IgM primary antibody (Carbosource) in blocking buffer in a sealed polypropylene envelope overnight at 4°C, washed 3 times with 1x TBST for 10 minutes, probed with goat anti-rat IgG H+L secondary antibody (Fisher, PI31629), washed twice with 1x TBST for 10 minutes, once

with 1x TBS for 10 minutes, treated with chemiluminescent substrate (Immobilon, WBKLS0500) and analyzed on CL-XPosure film (Fisher, 34090).

Pollen assays

All pollen germination and growth assays were carried out using *in vitro* pollen growth media (PGM) modified from Rodriguez-Enriquez et al. (2013) composed of 10% sucrose, 0.01% boric acid, 1mM $CaCl_2$, 1mM $Ca(NO_3)_2$, 1mM KCl, 0.03% casein enzymatic hydrolysate, 0.01% myo-inositol, 0.1 mM spermidine, 10mM γ-Aminobutyric acid, 500μM methyl jasmonate, pH adjusted to 8.0 and solidified with 1% low melting temperature agarose. The agarose was dissolved by slow heating on a 100°C stir plate and the media was poured into 35 mm petri plates. When solidified, the media was covered with a piece of cellophane. To germinate and grow PTs *in vitro*, pollen from recently opened flowers was dusted directly onto the cellophane and the PGM plates were placed in a humid chamber consisting of a plastic box with damp paper towels. For PT length measurements pollen was allowed to grow for five hours before tubes were imaged with a dissecting microscope equipped with a camera. PTs were measured using ImageJ. For PT width measurements PTs were imaged on a compound microscope using a 20X objective after 3 hours of growth *in vitro*. Three measurements were made across the width of each tube ≥ 10 μm from the pollen grain and tip using ImageJ. The measurements were averaged to generate a single width measurement per tube. To determine PT rupture frequency PTs were imaged after 3 hours of growth and the number of ruptured tubes was divided by the total number of PTs analyzed.

To measure PT growth rates, pollinated PGM plates were immobilized in 100 mm x 15 mm petri dishes with double-sided tape, and pieces of damp paper towel were placed in the larger petri dish to maintain high humidity. These plates were then placed directly on the stage of a dissecting microscope (equipped with a camera) and not moved for 3 hours of imaging. To determine sustained growth rates, images of the same field of PTs were taken at 20-minute intervals. PT lengths were measured at each time point, the change in length calculated and growth rate determined by dividing the number of minutes between images. The growth rates from every interval of every PT for each genotype was averaged to generate an overall “global” growth rate value. At

least 30 PTs were analyzed for each genotype. To determine the length of pre-rupture growth stalling in *hpat1/3* PTs, the above procedure was followed with the imaging interval reduced to 5 minutes and the time of rupture noted.

Protein extraction from pollen tubes and western blot analysis

Protein extraction from PTs was performed as described in Chang et al. (2017), with slight modifications. Flowers were collected in 1.5 ml microcentrifuge tubes and suspended in 1 ml agarose-free PGM. The tubes were vortexed for 1 minute and incubated at room temperature in the dark for 3-5 hours with agitation. Flower debris was removed with forceps and PTs were collected by centrifugation at 12,000 RPM for 2 minutes. The supernatant was removed and the pollen pellet tube was placed on ice. Using a polypropylene pestle, the pellet was ground for 1 minute and then incubated in K-HEPES protein extraction buffer buffer (20 mM HEPES, pH 7.0, 110 mM K-acetate, 2 mM $MgCl_2$, 0.1% Tween 20, 0.2% Triton X-100, 1 mM PMSF) for 1 hour on ice. The tubes were then centrifuged at 14,000 RPM for 20 minutes. The soluble fraction in the supernatant was removed and the insoluble fraction/pellet was resuspended 2x Laemmli sample buffer with β-mercaptoethanol, diluted 1:1 with K-HEPES buffer, and then heated to 95°C for 10 minutes. For western blots, the insoluble protein extract was separated by SDS-PAGE (15% polyacrylamide) and transferred onto a nitrocellulose membrane using the Trans-Blot® Turbo™ transfer system. Membranes were then blocked for 1.5 hours with 5% milk in 1x TBST, and probed with either 1:10 JIM20 monoclonal rat IgM primary antibody (Carbosource) or 1:1000 anti-GFP polyclonal rabbit IgG (Life Technologies) in blocking buffer in a sealed polypropylene envelope overnight at 4°C with agitation. The next day, membranes were washed 3 times with 1x TBST for 10 minutes, probed with either goat anti-rat HRP-conjugated secondary antibody (for JIM20) or anti-rabbit HRP-conjugated secondary antibody (for anti-GFP), sealed in a polypropylene envelope and incubated at room temperature for 1.5 hours with agitation. Membranes were then washed twice with 1x TBST for 10 minutes, once with 1x TBS for 10 minutes, treated with chemiluminescent substrate (SuperSignal West Femto Maximum Sensitivity Substrate) for 5 minutes and imaged with a LI-COR Odyssey Fc Dual-Mode Imaging System.

Cloning

For the transgenic rescue construct, the *EXO70A2* gene was amplified from Columbia-0 in a single fragment including the native promotor (376 bp), coding region and the 3' sequence up to the first predicted Polyadenylation site using the primers in Table S4 with Phusion® High-Fidelity DNA Polymerase (NEB, M0530S). For C-terminal fusion to mNeonGreen, the *EXO70A2* sequence was amplified from the promoter to the last coding codon from either Columbia-0 or the *exo70a2-2* mutant. The resulting fragments were cloned into Gateway® entry clones via BP Clonase II™ (Invitrogen, 11789-020). The transgenic rescue construct was recombined via LR Clonase II™ (Invitrogen, 11791-020) into the pFAST-G01 binary vector (Shimada, Shimada and Hara-Nishimura, 2010) and the localization reporters were recombined into a modified pFAST-R07 vector in which the GFP sequence was replaced with mNeonGreen. Due to restriction site limitations, a portion of the pFAST-R07 vector was amplified, using the Phusion® High-Fidelity DNA Polymerase (NEB, M0530S) alongside the mNeonGreen fusion protein, and the two fragments joined by overlap extension PCR. The GFP sequence was removed from pFAST-R07 by NruI and MluI restriction digestion and the mNeonGreen-containing fragment inserted using T4 DNA Ligase (Promega, M1801) to make pFAST-mNG.

The GF(EXT3)P construct was generated through the following steps. *pPS48-35SPro-GF-Muc1-P-35S-term* is an intermediate vector previously assembled for embed *GFP* cloning (Yang et al., 2012) where the signal sequence (*At*SS) was derived from the N-terminal signal peptide sequence of *A. thaliana* Basic endochitinase B (Uniprot: P19171). Firstly, the *GF-Muc1* fragment was obtained by *PstI*/*BamHI* double digestion and used as template for PCR with primers FReplace and RReplace. The resulting GF-Muc1 fragment was cloned into the multiple cloning site of pPS48. The two EXT3 encoding oligos, pYi1 and pYi2 were inserted into the NcoI/BamHI site of pPS48 vector. The entire fragment CaMV35S-*At*SS-GF(EXT3)P-NosTerm was excised using *XbaI* and ligated into pGreen0179, yielding the plant expression plasmid pGreen0179-35SPro-*At*SS-GF(EXT3)P-NosTerm. The *At*SS sequence in this construct was substituted with the signal sequence of EXT3 (At1g21310) by an In-Fusion cloning

(Takara #638933), using the primer sets p162 and p164 on *35SPro-At*SS-*GF(EXT3)P-NosTerm* to obtain the fragment containing the 35S promoter from pGreen and EXT3 signal peptide overlap and the primer set p163 and p165 on *35SPro-AtSS-GF(EXT3)P-NosTerm* to obtain signal peptide overlap, imbed GFP and 35S terminator. The vector fragment was obtained from V26 (pUC57, including Synthetic gene fragments and AttL sites, obtained from Genescript) digested with SpeI and XbaI for directed insertion of *35SPro-EXT3ss* and *EXT3ss-GF(EXT3)P-NosTerm* into the vector fragment using the In-Fusion Cloning kit. The LAT52 promoter for pollen expression was amplified from tomato genomic DNA using the primers in Table S4. The EXT3ssGF(Ext3)P fragment was amplified from the *EXT3ss-GF(EXT3)P-NosTerm* plasmid, incorporating attB2 and attB5 sites in the forward and reverse primers, respectively (GF(EXT3)P F and GF(EXT3)P R). The LAT52pro and EXT3ssGF(EXT3)P fragments were cloned into their respective Gateway® entry vectors via BP Clonase II™ (Invitrogen, 11789-020). The LAT52pro and EXT3ssGF(EXT3)P entry clones were combined with the pFAST-G01 vector (Shimada, Shimada and Hara-Nishimura, 2010) by two-fragment recombination using LR Clonase II™ (Invitrogen, 11791-020). The control LAT52:GFP construct was generated by one-fragment LR Clonase II™ (Invitrogen, 11791-020) recombination between a LAT52pro entry vector and pFAST-G07, which contains the GFP coding sequence (Shimada, Shimada and Hara-Nishimura, 2010).

Microscopy

For immunolocalization, PTs were fixed, imaged and analyzed as described in Chebli et al. 2012, with several modifications. PTs were grown in agarose-free PGM for at least 2 hours, then the media with PTs was transferred to a 12 x 75mm polystyrene culture test tube. PTs were collected by centrifugation at 1000 rpm for 2 minutes with low acceleration and deacceleration and the growth media was removed. For fixation, PTs were resuspended in 3.5% formaldehyde in PIPES buffer (50 mM PIPES, 1 mM EGTA, 5 mM $MgSO_4$, 0.5 mM $CaCl_2$, pH 7) and vacuum infiltrated for 20 minutes. After fixation, PTs were washed three times with PIPES buffer and then three times with PBS + 3% BSA. After the final wash, PTs were resuspended in primary antibody and incubated at 4°C overnight with gentle agitation. Primary antibodies were diluted in PBS

+ BSA to the following concentrations: JIM20- 1:5, LM19- 1:10, LM20- 1:5 (antibodies obtained from PlantProbes). The next day, the tubes were spun and down and primary antibody was removed, and PTs were washed three times in PBS + BSA. Anti-rat-FITC-conjugated secondary antibody (diluted 1:100 in PBS + BSA), was added, and the tubes were incubated at room temperature in the dark for 2 hours. After incubation, PTs were washed three times with PBS followed by three washes with DI water. PTs were then resuspended in mounting media (0.1% gelatin and 10% ethanol), transferred to slides with a pipette, and slides were stored overnight in the dark at room temperature to allow PTs to settle onto the mounting media. The next day, VectaShield was added to the slides, covered with a #1.5 coverslip, sealed with nail polish, and stored at 4^{o} C.

Imaging was performed with a Leica SP5 laser-scanning confocal microscope. To image FITC signal, we used a 488 nm excitation laser, an RSP 500 dichroic beam splitter, and detectors were set to capture light with a wavelength range of 495-600 nm. For each different experiment, the imaging settings including laser intensity, gain, line averaging and frame accumulation were adjusted so that the signal from the overall brightest tube was just below saturation; all images for a single experiment were taken with identical settings. Z stacks were taken throughout the entire volume of each PT. Z slice step sizes were automatically optimized and maximum intensity projections were generated using LAS-AF software. N ≥ 30 PTs for each genotype. Images were analyzed using ImageJ. To measure fluorescence signal intensities, a line was drawn using the segmented line tool along the periphery of the PT starting from the center of the PT tip towards the pollen grain, or as far as the possible. Two measurements were performed for each PT along each periphery/side. ImageJ's "Plot profile" tool was used to measure pixel grey value along distance, with distance = 0 representing the tip apex. For a single PT, the values of each side were averaged to generate a single measurement, and the measurements of all PTs were averaged within each genotype.

For aniline blue staining, PTs were grown *in vitro* on PGM plates with cellophane for 2 hours. A drop of 0.1 mg/ml aniline blue fluorochrome (ABFC, Biosupplies Australia Pty. Ltd.) diluted 1:70 in 0.1 M KH_2PO_4, pH 10 was added to a microscope slide, and PTs were transferred to the slide by dabbing the cellophane on the ABFC solution. Nail polish was applied to the slide surrounding the PTs and a coverslip was mounted onto

the nail polish. PTs were imaged with a Leica SP5 laser-scanning confocal microscope, using a UV excitation laser with 405 nm wavelength, a Substrat dichroic beam splitter, and detectors were set to capture light with 411-502 nm wavelengths. Image acquisition and analysis was carried out as above for immunolocalization.

For imaging of EXO70A2-mNG fusions PTs were grown *in vitro* on PGM plates with cellophane for 2 hours. After growth time, the cellophane was transferred to a slide and a drop of agarose-free PGM with 4 μM FM4-64 was added on top of the cellophane and PTs. Nail polish was applied to the slide and a coverslip was added on top of the nail polish, covering the liquid media. PTs were imaged using a Leica SP5 laser-scanning confocal microscope 10 minutes after FM4-64 application. To image EXO70A2-mNG, we used an excitation laser with 488 nm wavelength, a RSP500 dichroic beam splitter, and detectors were set to capture light with a wavelength range of 494-575 nm. To image FM4-64, we used an excitation laser with 514 nm wavelength, a DD 458/514 dichroic beam splitter, and detectors were set to capture light with a wavelength range of 620-783 nm.

To analyze secretion of the GF(EXT3)P reporter, PTs were grown for 1-2 hours under normal *in vitro* conditions on PGM plates with a layer of cellophane. To induce plasmolysis, PTs were transferred to PGM plates containing 25% sucrose (vs. 10% for standard plates), without cellophane. Plasmolysis could be observed within a few minutes of transfer. Plasmolyzed PTs that were expressing GF(EXT3)P were imaged at 40x magnification using a Leica DM5500 compound microscope. To measure fluorescent signal intensity at the plasmolyzed cell wall region, a region of interest (ROI) was drawn in the entire plasmolyzed region using the differential interference contrast (DIC) channel, excluding the plasma membrane boundary. This ROI was then added to the fluorescent channel and mean fluorescence intensity was measured. For the cytoplasm measurements, two ROIs approximately 5 μm^2 were selected about 10-20 μm from the plasma membrane, and the mean fluorescence intensities of each cytoplasmic ROI were averaged. The average of three background measurements was subtracted from both the cell wall and cytoplasm measurements. The secretion index (SI) was calculated as the ratio of cell wall/cytoplasm signal. A minimum of 30 tubes per

genotype were measured and statistical significance was determined using the Benjamini–Hochberg False Discovery Rate with FDR = 0.05.

Data Availability Statement

High-throughput sequence data is available from the NCBI Sequence Read Archive (https://www.ncbi.nlm.nih.gov/Traces/study/?) under project accession number PRJNA574113. All other material and data are available upon request from the corresponding author.

Acknowledgments

This material is based upon work supported by the National Science Foundation under Grant No. IOS-1755482. This work was also supported by the Danish Councils for Strategic and Independent Research (12-125709, 12-131859) and the Copenhagen University Excellence Program for Interdisciplinary Research (CDO2016). We wish to thank Gregg Sobocinski for microscopy assistance and advice.

Author Contributions

Cora MacAlister designed the study, conducted the *frh* mutant screen and wrote the paper. Steven Beuder carried out all immunofluorescence, microscopy, bioinformatic analysis of whole genome sequences to identify candidate suppressor mutations, functional rescue assays, and performed crosses and PT phenotyping. Bent L. Petersen and Svenning Rune Moeller generated the 35S::EXT3ssGF(EXT3)P construct and the *rra2/3* double mutant. Alexandria Dorchak carried out all other cloning and the JIM20 dot blot and western blots. Ashwini Bhide conducted genotyping and genetic co-segregation experiments. All authors edited the manuscript.

Conflicts of Interest

The authors declare no conflicts of interest.

Supporting Material Legends

Fig. S1- frh1 suppresses most, but not all hpat1/3 pollen tube phenotypes

A-C) Differential interference contrast (DIC) images of PT phenotypic classes. A) a morphologically normal PT typical of the wild type, B) a ruptured PT and C) a "branched" PT typical of *hpat1/3* mutants. D) Time course of an *hpat1/3* branching event imaged at 5-minute intervals. White arrow marks the original tip region; black arrow marks the newly formed tip derived from a sub-apical portion of the PT. E) Frequency of *in vitro* pollen germination after 3 hours of growth. Pollen were considered germinated if a visible tube of at least one half the length of the pollen grain was identifiable. Note that the reduced germination in *hpat1 hpat3* is in part due to their poor tube elongation. N>600 per genotype. F) Frequency of PT rupture for the indicated genotypes. No ruptured tubes were observed in WT. N>500 per genotype. G) Percentage of tubes with two morphologically distinct tip regions after 5 hours of *in vitro* PT growth. N>200 per genotype. H) Average PT widths (±SD, N ≥ 103 for each genotype). I) PT growth rates. Asterisks in H and I mark statistically significant T-test p-values; '*' indicates p-value ≤0.05 and '***' indicates p-value ≤0.0005.

Fig. S2- The JIM20 monoclonal antibody recognizes Hyp-Ara

A) Illustration of the Hyp-Ara modification and the enzymes responsible for the addition of each arabinose. B) The EXT antibody JIM20 requires Hyp substituted with at least three arabinoses, i.e. the presence of the HPAT, RRA and XEG113 enzymes, for recognition. Dot blot and SDS-PAGE Western blot analysis of protein isolated from seedlings (top, Dot blot) or extracted from rosette leaves (bottom, Western blot) of the indicated genotypes and probed JIM20. C-E) JIM20 immunostaining visualized with a FITC-conjugated secondary antibody (left) of PTs (top) and pollen grains (bottom) compared to the corresponding DIC images (right). Images taken at 20x magnification. C) Wild-type Columbia-0 pollen samples produced robust JIM20 signal in both pollen grains and PTs, particularly near the PT tip. D) Secondary antibody alone control staining did not produce detectable signal. E) In *hpat1/3* pollen samples no JIM20 signal

was detected. F) *frh1 hpat1/3* and *hpat1/3* pollen displayed similar appearance with no detectable JIM20 signal. All immunolocalizations were imaged using the same light intensity and exposure settings.

Fig. S3- Alignment of Arabidopsis EXO70 protein sequences in the region of the exo70a2-2 G319E mutation

Clustal Omega multiple sequence alignment of the whole proteins sequences were trimmed to the region of interest. The EXO70A2 G319 position is marked with red highlight. Conserved residues are marked with "*", ":" marks positions with conservation of amino acids with strongly similar properties, "." marks conservation between weakly similar amino acid properties.

Fig. S4- The exo70a2-2 mutations co-segregates with the frh1 suppressive phenotype

A) PCR and restriction enzyme mediated genotyping of 20 *frh1* BC5 F2 individuals visualized on an agarose gel. The *exo70a2-2* mutation creates a TaqαI restriction enzyme recognition site. The upper band is the un-cut wild-type product and the lower band is the cleaved *exo70a2-2* product. The two individuals with a non-suppressed phenotype are marked by '*' and both are homozygous WT. B) Table of the *exo70a2-2* genotype distribution for 123 *frh1* BC5 F2 plants. The 11 wild-type individuals (+/+) were all non-suppressed, all remaining plants (heterozygous, +/-; homozygous mutant, -/-) were phenotypically suppressed. Note also the significant distortion of genotype ratio compared to the Mendelian 25%:50%:25% ratio (chi-squared p-value = 2.42×10^{-7}). This bias against the recovery of homozygous wild-type plants is consistent with the genetic behavior of *frh1*. C) Average number of seeds per silique (+/- SD, N≥16) in the BC5 F2 population grouped by *exo70a2-2* genotype. Asterisks mark statistically significant T-test p-values, '**' indicates p-value ≤0.005 and '***' indicates p-value ≤0.0005.

***Fig. S5-* frh1 *suppression is due to a mutation in* exo70a2**

A) *frh1 hpat1/3* plants were transformed with a rescue construct containing the wild-type genomic EXO70A2 region and seed-expressed fluorescence reporter selection cassette

(*OLE1-GFP*; Shimada, Shimada and Hara-Nishimura, 2010). Transgene transmission efficiency (TE) for three independent hemizygous single loci insertion transgenic lines. '**' marks significant difference from the expected TE for no effect of the transgene on transmission (100%, T-test P-value <0.005, N≥185). B) Transmission of a control construct containing the strong pollen promoter (Lat52) driving expression of the fluorescent protein mNeonGreen in four independent *frh1 hpat1/3* lines (N≥72). C) Seed counts of T3 plants segregating for the rescue construct. Plants not carrying the rescue construct (0/0) maintained suppressor-levels of seed set. Seed set of plants homozygous for the presence of the rescue construct (+/+) was not statistically different from the *hpat1/3* background ('***' indicates p-value < 0.0005; Student's T-test vs. *hpat1/3;* N ≥ 15 siliques).

Fig. S6- exo70a2-2 PTs maintain cell wall polymer polarity in the WT background
A) Medial Z-slices of PTs stained with LM19 primary antibody and anti-rat FITC-conjugated secondary antibody, and corresponding quantification of fluorescent signal intensity along the PT periphery, starting at the tip (distance on x-axis = 0 μm) to 25 μm down the shaft. B) Medial Z-slices of PTs stained with LM20 primary antibody and anti-rat FITC-conjugated secondary antibody, and corresponding quantification of fluorescent signal intensity as in (A). C) Maximum projections of PTs stained with aniline blue fluorochrome (ABF) and corresponding quantification of fluorescent signal intensity starting at the tip (distance on x axis= 0) to 50 μm down the shaft of the PT. D) Medial Z-slices of PTs stained with JIM20 primary antibody and anti-rat FITC-conjugated secondary antibody, and corresponding fluorescent signal quantification as in (A) and (B). Colored lines represent means and shading represents standard error. Vertical dashed line represents the approximate region of the PT where the apical dome transitions to the shaft. N ≥ 30 PTs for each genotype per experiment. All images were acquired by confocal microscopy at 100x magnification and all scale bars = 10 μm.

Fig. S7- EXO70A2-mNG rescues pollen tube germination in the exo70a2-3 mutant.
A) PTs were grown *in vitro* for 2 hours and imaged with GFP filter (left) and DIC optics (right). Wild-type un-transformed Columbia are shown as a negative control for

fluorescence. B) pollen germination frequency in *exo70a2-3.* The presence of EXO70A2-mNG significantly increased pollen germination compared to the background. The point mutant allele EXO70A2-2 (G319E) also increased pollen germination to a smaller degree. Each point is data from a single independent T1 plant, N ≥ 321 pollen grains per T1. '***' indicates p-value < 0.0005, '**' indicates p-value < 0.005, '*' indicates p-values < 0.05. C) Percentage of fluorescent PTs for *exo70a2-3* EXO70A2-mNG hemizygous lines.

Table S1- Illumina sequencing read information

DNA samples of the indicated genotype, all in the *hpat1/3* background, were sequenced by paired-end Illumina sequencing. At least 97% of reads aligned to the Columbia reference genome yielding estimated genome coverage between 18 and 63 fold.

Table S2- Full list of sequence variants passing filtering for frh1

AO- alternate observations (number of reads with the alternative nucleotide), RO- reference observations (number of reads carrying the reference nucleotide), TO- total observations (AO + RO). Allele frequency is estimated from reads as (AO/TO). Gene function, annotations for missense mutations are show in black; silent, UTR or intronic mutations are in grey. Double lines separate chromosomes. The *exo70a2* mutation is in bold.

Table S3- Full list of sequence variants passing filtering for frh2

AO- alternate observations (number of reads with the alternative nucleotide), RO- reference observations (number of reads carrying the reference nucleotide), TO- total observations (AO + RO). Allele frequency is estimated from reads as (AO/TO). Gene function, annotations for missense mutations are show in black; silent, UTR or intronic mutations are in grey. Double lines separate chromosomes. The *sec15a* mutation is in bold.

Table S4- Primers used in this study

References

Alonso JM, Stepanova AN, Leisse TJ, Kim CJ, Chen H, Shinn P, Stevenson DK, Zimmerman J, Barajas P, Cheuk R, Gadrinab C, Heller C, Jeske A, Koesema E, Meyers CC, Parker H, Prednis L, Ansari Y, Choy N, Deen H, Geralt M, Hazari N, Hom E, Karnes M, Mulholland C, Ndubaku R, Schmidt I, Guzman P, Aguilar-Henonin L, Schmid M, Weigel D, Carter DE, Marchand T, Risseeuw E, Brogden D, Zeko A, Crosby WL, Berry CC, Ecker JR. (2003) Genome-wide insertional mutagenesis of Arabidopsis thaliana. Science 301: 653-657.

Anderson CT (2015) We be jammin': an update on pectin biosynthesis, trafficking and dynamics. J Experimental Botany 67: 495-502.

Bate, N. and Twell, D. (1998). Functional architecture of a late pollen promoter: pollen-specific transcription is developmentally regulated by multiple stage-specific and co-dependent activator elements. Plant Mol. Biol. 37: 859–69.

Beuder S and MacAlister CA. Isolation and cloning of suppressor mutants with improved pollen fertility (2020) In: Pollen and Pollen Tube Biology: Methods and Protocols, Anja Geitmann (editor) MIMB, Humana Press, IN PRESS

Bloch D, Pleskot R, Pejchar P, Potocký M, Trpkošová P, Cwiklik L, Vukašinović N, Sternberg H, Yalovsky S, Žárský V (2016) Exocyst SEC3 and phosphoinositides define sites of exocytosis in pollen tube initiation and growth. Plant Physiology 172: 980-1002

Borassi C, Sede AR, Mecchia MA, Salter JDS, Marzol E, Muschietti JP, Estevez JM (2016) An update on cell surface proteins containing extensin-motifs. J Experimental Botany 67: 477-487

Bosch M and Hepler PK (2005) Pectin methylesterases and pectin dynamics in pollen tubes. Plant Cell 17: 3219-3226.

Bove J, Vaillancourt B, Kroeger J, Hepler PK, Wiseman PW and Geitmann A (2008). Magnitude and direction of vesicle dynamics in growing pollen tubes using spatiotemporal image correlation spectroscopy and fluorescence recovery after photobleaching. Plant Physiol. 147: 1646–1658.

Brownleader, M.D. and Dey P.M. (1993) Purification of extensin from cell walls of tomato (hybrid of Lycopersicon esculentum and L. peruvianum) cells in suspension culture. Planta 191: 457-469

Campanoni, P., and Blatt, M.R. (2007). Membrane trafficking and polar growth in root hairs and pollen tubes. J. Exp. Bot. 58: 65–74.

Cannon MC, Terneus K, Hall Q, Tan L, Wang Y, Wegenhart BL, Chen L, Lamport DTA, Chen Y, Kieliszewski MJ (2008) Self-assembly of the plant cell wall requires an extensin scaffold. Proc Natl Acad Sci USA 105: 2226–2231

Chang, M and Huang, S (2017) Rapid Isolation of Total Protein from *Arabidopsis* Pollen. *Bio-protocol* 7(8): e2227. DOI: 10.21769/BioProtoc.2227.

Chebli Y, Kaneda M, Zerzour R, Geitmann A (2012) The cell wall of the Arabidopsis pollen tube –spatial distribution, recycling, and network formation of polysaccharides. Plant Physiology 160: 1940–1955.

Chen, Y., Dong, W., Tan, L., Held, M.A., and Kieliszewski, M.J. (2015). Arabinosylation plays a crucial role in extensin cross-linking in vitro. Biochem. Insights 8: 1–13.

Cheung, A.Y., Niroomand, S., Zou, Y., and Wu, H.-M. (2010). A transmembrane formin nucleates subapical actin assembly and controls tip-focused growth in pollen tubes. Proc. Natl. Acad. Sci. U. S. A. 107: 16390–5.

Cheung, A.Y. and Wu, H. (2004). Overexpression of an Arabidopsis formin stimulates supernumerary actin cable formation from pollen tube cell membrane. Plant Cell 16: 257–269.

Chong YT, Gidda SK, Sanford C, Parkinson J, Mullen RT and Goring DR (2009) Characterization of the Arabidopsis thaliana exocyst complex gene families by phylogenetic, expression profiling, and subcellular localization studies. New Phytologist 185:401-419

Choudhary P, Saha P, Ray T, Tang Y, Yang D and Cannon MC (2015) *EXTENSIN18* is required for full male fertility as well as normal vegetative growth in Arabidopsis. Frontiers in Plant Sci. 6: 553

Cole RA, Synek L, Zarsky V and Fowler JE (2005) SEC8, a subunit of the putative Arabidopsis Exocyst complex, facilitates pollen germination and competitive pollen tube growth. Plant Physiol. 138: 2005-2018.

Cole RA, McInally SA and Fowler JE (2014) Developmentally distinct activities of the exocyst enable rapid cell elongation and determine meristem size during primary root growth in Arabidopsis. BMC Plant Biology 14: 386

Cosgrove DJ (2005) Growth of the plant cell wall. Nature Reviews Molecular Cell Biology 6: 850–861

Dardelle F, Lehner A, Ramdani Y, Bardor M, Lerouge P, Driouich A, Mollet JC (2010) Biochemical and immunocytological characterizations of Arabidopsis pollen tube cell wall. Plant Physiol. 153: 1563-1576.

Fendrych M, Synek L, Pečenková T, Toupalová H, Cole R, Drdová E, Nebesářová J, Šedinová M, Hála M, Fowler JE, Žárský V (2010) The Arabidopsis Exocyst complex is involved in cytokinesis and cell plate maturation. Plant Cell 22: 3053-3065.

Fry SC (1988) *The Growing Plant Cell Wall: Chemical and Metabolic Analysis*. Longman Scientific & Technical, UK.

Grobei MA, Qeli E, Brunner E, Rehrauer H, Zhang R, Roschitzki B, Basler K, Ahrens CH and Grossniklaus U (2009) Deterministic protein inference for shotgun proteomics data provides new insights into Arabidopsis pollen development and function. Genome Res. 19: 1786-1800.

Hála M, Cole R, Synek L, Drdová E, Pečenková T, Nordheim A, Lamkemeyer T, Madlung J, Hochholdinger F, Fowler JE, Žárský V (2008) Exocyst complex functions in plant cell growth in Arabidopsis and tobacco. Plant Cell 20: 1330-1345.

Harsay E and Bretscher A (1995) Parallel secretory pathways to the cell surface in yeast. J Cell Biol. 131: 297-310.

He B, Xi F, Zhang X, Zhang J, Guo W (2007a) Exo70 interacts with phospholipids and mediates the targeting of the exocyst to the plasma membrane. EMBO J. 26:4053-4065.

He B, Xi F, Zhang J, TerBush D, Zhang X and Guo W (2007b) Exo70p mediates the secretion of specific exocytic vesicles at early stages of the cell cycle for polarized cell growth, J Cell Biol. 176: 771-777.

Helm, M, Schmid M, Hierl G, Terneus K, Tan L, Lottspeich F, Kieliszewski MJ and Gietl C (2008) KDEL-tailed cysteine endopeptidases involved in programmed cell death, intercalation of new cells, and dismantling of extensin scaffolds. Am. J. Botany 95: 1049-1062.

Hepler, P.K., Vidali, L., and Cheung, A.Y. (2001). Polarized cell growth in higher plants. Annu. Rev. Cell Dev. Biol. 17: 159–87.

Hepler PK, Rounds CM and Winship LJ (2013) Control of cell wall extensibility during pollen tube growth. Mol Plant 6: 998-1017

Hill AE, Shachar-Hill B, Skepper JN, Powerll A and Shachar-Hill Y (2012) An osmotic model of the growing pollen tube. PLoS ONE 7: e36585.

Hruz, T., Laule, O., Szabo, G., Wessendorp, F., Bleuler, S., Oertle, L., Widmayer, P., Gruissem, W., and Zimmermann, P. (2008). Genevestigator v3: a reference expression database for the meta-analysis of transcriptomes. Adv. Bioinformatics 2008: 420747.

Imin N, Patel N, Corcilius L, Payne RJ, Djordjevic MA (2018) CLE peptide tri-arabinosylation and peptide domain sequence composition are essential for SUNN-dependent autoregulation of nodulation in Medicago truncatula. New Phytol. 218: 73-80.

Johnson KL, Cassin AM, Lonsdale A, Bacic A, Doblin MS, and Schultz CJ (2017) Pipeline to identify Hydroxyproline-Rich Glycoproteins. Plant Physiol. 174: 886–903.

Kalmbach L, Hématy K, De Bellis D, Barberon M, Fujita S, Ursache R, Daraspe J and Geldner N. (2017) Transient cell-specific EXO70A1 activity in the CASP domain and Casparian strip localization. Nature Plants 3: 17058.

Kanaoka and Higashiyama (2015) Peptide signaling in pollen tube guidance. Current opinion in plant biology 28: 127-136

Kassaw T, Nowak S, Schnabel E, Frugoli J (2017) ROOT DETERMINED NODULATION1 is required for M. truncatula CLE12, but not CLE13, peptide signaling through the SUNN receptor kinase. Plant Physiol. 174: 2445-2456

Kieliszewski, M.J. and Shpak, E. (2001). Synthetic genes for the elucidation of glycosylation codes for arabinogalactan-proteins and other hydroxyproline-rich glycoproteins. Cell. Mol. Life Sci. 58: 1386–1398.

Klepikova AV, Kasianov AS, Gerasimov ES, Logacheva MD, Penin AA (2016) A high resolution map of the Arabidopsis thaliana developmental transcriptome based on RNA-seq profiling. Plant J. 88: 1058-1070.

Kulich I, Cole R, Drdová E, Cvrčková F, Soukup A, Fowler J, Žárský V (2010) Arabidopsis exocyst subunits SEC8 and EXO70A1 and exocyst interactor ROH1 are involved in the localized deposition of seed coat pectin. New Phytol. 188: 615-625

Kulich I, Vojtíková Z, Sabol P, Ortmannová J, Neděla V, Tihlaříková E and Žárský V (2018) Exocyst subunit EXO70H4 has a specific role in callose synthase secretion and silica accumulation. Plant Physiol. 176: 2040-2051.

Kulich, I., Vojtíková, Z., Glanc, M., Ortmannová, J., Rasmann, S., Žárský, V. (2015) Cell wall maturation of Arabidopsis trichomes is dependent on Exocyst subunit EXO70H4 and involves callose deposition. Plant Physiol. 168: 120-131

Lamport, D.T.A. and Miller, D.H. (1971). Hydroxyproline Arabinosides in the Plant Kingdom. Plant Physiol. 48: 454–456.

Lamport, D.T.A. (1967). Hydroxyproline-O-glycosidic Linkage of the Plant Cell Wall Glycoprotein Extensin. Nature 216: 1322–1324.

Le Y, Tan X, Wang M, Li B, Zhao Y, Wu C, Rui Q, Wang J, Liu Z, Bao Y (2017) Exocyst subunit SEC3A marks the germination site and is essential for pollen germination in Arabidopsis thaliana. Sci Rep. 7: 40279

Leucci MR, Sansebastiano, PD, Gigante M, Dalessandro G and Piro G (2007) Secretion marker proteins and cell-wall polysaccharides move through different secretory pathways. Planta 225: 1001-1017

Li Y, Tan X, Wang M, Li B, Zhao Y, Wu C, Rui Q (2017) Exocyst subunit SEC3A marks the germination site and is essential for pollen germination in Arabidopsis thaliana. Sci Rep. 7: 40279.

Li S, Chen M, Yu D, Ren S, Sun S, Liu L, Ketelaar T, Emons AM, Liu CM (2013) EXO70A1-mediated vesicle trafficking is critical for tracheary element development in Arabidopsis. Plant Cell 25: 1774-1786.

Li S, van Os GM, Ren S, Yu D, Ketelaar T, Emons AM, Liu CM (2010) Expression and functional analyses of EXO70 genes in Arabidopsis implicate their roles in regulating cell type-specific exocytosis. Plant Physiol. 154: 1819-1830

Liu J, Zuo X, Yue P, Guo W (2007) Phosphatidylinositol 4,5-bisphosphate mediates the targeting of the exocyst to the plasma membrane for exocytosis in mammalian cells. Mol. Biol. Cell.18: 4483–4492.

Liu X, Wolfe R, Welch LR, Domozych DS, Popper ZA, Showalter AM (2016) Bioinformatic identification and analysis of Extensins in the plant kingdom. PLoS One 11(2): e0150177

MacAlister, C.A., Ortiz-Ramírez, C., Becker, J.D., Feijó, J.A., and Lippman, Z.B. (2016). Hydroxyproline O-arabinosyltransferase mutants oppositely alter tip growth in Arabidopsis thaliana and Physcomitrella patens. Plant J. 85: 193–208.

Marković V, Cvrčková F, Potocký M, Pejchar P, Kollárová E, Kulich I, Synek L, Žárský V (2019) EXO70A2 is critical for the exocyst complex function in Arabidopsis pollen. bioRxiv doi: 10.1101/831875

McKenna ST, Kunkel JG, Bosch M, Rounds CM, Vidali L, Winship LJ and Hepler PK (2009). Exocytosis precedes and predicts the increase in growth in oscillating pollen tubes. Plant Cell 21: 3026-3040.

Micheli F (2001). Pectin methylesterases: cell wall enzymes with important roles in plant physiology. Trends Plant Sci. 6: 414-419.

Mei K and Guo W (2018) The exocyst complex. Curr Biol 28: R922-R925

Ogawa-Ohnishi, M., Matsushita, W., and Matsubayashi, Y. (2013). Identification of three hydroxyproline O-arabinosyltransferases in Arabidopsis thaliana. Nat. Chem. Biol. 9: 726–730.

Ohyama K, Shinohara H, Ogawa-Ohnishi M, Matsubayashi Y. (2009) A glycopeptide regulating stem cell fate in Arabidopsis thaliana. Nat Chem Biol. 5:578-80.

Peterson R, Sloven JP and Chen C (2010) A simplified method for differential staining of aborted and non-aborted pollen grains. International Journal of Plant Biology 1: e13

Qi X, Behrens BX, West PR, Mort AJ. (1995) Solubilization and partial characterization of extensin fragments from cell walls of cotton suspension cultures. Evidence for a covalent cross-link between extensin and pectin. Plant Physiol. 108: 1691-701.

Rounds CM, Lubeck E, Hepler PK, Winship LJ (2011) Propidium iodide competes with Ca(2+) to label pectin in pollen tubes and Arabidopsis root hairs. Plant Physiology 157: 175–187.

Rybak K, Steiner A, Synek L, Klaeger S, Kulich I, Facher E, Wanner G, Kuster B, Zarsky V, Persson S, Assaad FF (2014) Plant cytokinesis is orchestrated by the sequential action of the TRAPPII and Exocyst tethering complexes. Developmental Cell 29: 607-620

Safavian D, Zayed Y, Indriolo E, Chapman L, Ahmed A, Goring D (2015) RNA silencing of exocyst genes in the stigma impairs the acceptance of compatible pollen in Arabidopsis. Plant Physiol. 169: 2526-2538.

Saha P, Ray T, Tang Y, Dutta I, Evangelous NR, Kieliszewski MJ, Chen Y, Cannon MC (2013). Self-rescue of an EXTENSIN mutant reveals alternative gene expression programs and candidate proteins for new cell wall assembly in Arabidopsis. 75: 104-116

Samuel MA, Chong YT, Haasen KE, Aldea-Brydges MG, Stone SL, Goring DR (2009) Cellular pathways regulating responses to compatible and self-incompatible

pollen in Brassica and Arabidopsis stigmas intersect at Exo70A1, a putative component of the Exocyst complex. Plant Cell 21: 2655-2671.

Schnabel EL, Kassaw TK, Smith LS, Marsh JF, Oldroyd GE, Long SR, Frugoli JA (2011) The ROOT DETERMINED NODULATION1 gene regulates nodule number in roots of Medicago truncatula and defines a highly conserved, uncharacterized plant gene family. Plant Physiol. 157:328-40

Sekereš J, Pejchar P, Šantrůček J, Vukašinović N, Žárský V, Potocký M (2017) Analysis of Exocyst subunit EXO70 family reveals distinct membrane polar domains in tobacco pollen tubes. Plant Physiol. 173: 1659-1675.

Shaner NC, Lambert GG, Chammas A, Ni Y, Cranfill PJ, Baird MA, Sell BR, Allen JR, Day RN, Israelsson M, Davidson MW, Wang J (2013) A bright monomeric green fluorescent protein derived from Branchiostoma lanceolatum. Nat Methods. 10:407-409.

Shimada TL, Shimada T and Hara-Nishimura I (2010) A rapid and non-destructive screenable marker, FAST, for identifying transformed seeds of Arabidopsis thaliana. Plant J. 61: 519-528.

Showalter AM, Keppler B, Lichtenberg J, Gu D and Welch LR (2010) A bioinformatics approach to the identification, classification, and analysis of hydroxyproline-rich glycoproteins. Plant Physiol. 153: 485-513.

Showalter AM and Basu D (2016) Extensin and arabinogalactan-protein biosynthesis: glycosyltransferases, research challenges, and biosensors. Front. Plant Sci. 7: 814

Sinclair R, Rosquete MR and Drakakaki G (2018) Post-Golgi trafficking and transport of cell wall components. Front. Plant Sci. 9: 1784.

Smith MM and McCully ME (1978) A critical evaluation of the specificity of Aniline Blue induced fluorescence. Protoplasma 95: 229-254

Stafstrom, J and Staehelin LA (1986a) Cross-linking patterns in salt-extractable extensin from Carrot cell walls. Plant Physiol 81: 234-241

Stafstrom JP, Staehelin LA (1986b) The role of carbohydrate in maintaining extensin in an extended conformation. Plant Physiol 81: 242–246

Synek L, Schlager N, Eliáš M, Quentin M, Hauser MT and Žárský V (2006). AtEXO70A1, a member of a family of putative exocyst subunits specifically expanded in land plants, is important for polar growth and plant development. Plant J. 48: 54-72.

Synek L, Vukašinović N, Kulich I, Hála M, Aldorfová K, Fendrych M, Žárský V (2017) EXO70C2 is a key regulatory factor for optimal tip growth of pollen. Plant Physiol. 174: 223-240.

Tan L, Varnai P, Lamport DTA, Yuan C, Xu J, Qiu F, Kieliszewski MJ (2010) Plant O-Hydroxyproline arabinogalactans are composed of repeating trigalactosyl subunits with short bifurcated side chains. J Biol. Chem. 285: 24575-24583

van Holst, G.J. and Varner, J.E. (1984). Reinforced Polyproline II Conformation in a Hydroxyproline-Rich Cell Wall Glycoprotein from Carrot Root. Plant Physiol. 74: 247–51.

Verhertbruggen Y, Marcus SE, Haeger A, Ordaz-Ortiz JJ, Knox JP (2009) An extended set of monoclonal antibodies to pectic homogalacturonan. Carbohydrate Research 344: 1858-1862.

Vukašinović N, Žárský V (2016) Tethering complexes in the Arabidopsis endomembrane system. Front Cell Dev Biol. 4: 46.

Wang J, Ding Y, Wang J, Hillmer S, Miao Y, Lo SW, Wang X, Robinson DG, Jiang L (2010) EXPO, an exocyst-positive organelle distinct from multivesicular endosomes and autophagosomes, mediates cytosol to cell wall exocytosis in Arabidopsis and tobacco cells. Plant Cell 22: 4009-4030

Williams, J.H., Edwards, J.A., and Ramsey, A.J. (2016). Economy, efficiency, and the evolution of pollen tube growth rates. Am. J. Bot. 103: 471–483.

Woody ST, Austin-Phillips S, Amasino RM, Krysan PJ (2007) The WiscDsLox T-DNA collection: an Arabidopsis community resource generated by using an improved high-throughput T-DNA sequencing pipeline. J Plant Res. 120: 157-165.

Xiang Y, Zhang X, Nix DB, Katoh T, Aoki K, Tiemeyer M and Wang Y (2012) Regulation of protein glycosylation and sorting by the Golgi matrix proteins GRASP55/65. Nature Comm. 4:1659.

Xu, C., Liberatore, K.L., MacAlister, C.A., Huang, Z., Chu, Y.-H., Jiang, K., Brooks, C., Ogawa-Ohnishi, M., Xiong, G., Pauly, M., Van Eck, J., Matsubayashi, Y., van der Knaap, E. and Lippman, Z.B. (2015) A cascade of arabinosyltransferases controls shoot meristem size in tomato. Nat. Genet., 47, 784–792.

Yang Z, Bennett EP, Jørgensen B, Drew DP, Arigi E, Mandel U, Ulvskov P, Levery SB, Clausen H, and Petersen BL (2012) Toward stable genetic engineering of human O-glycosylation in plants. Plant Physiol 160: 450-463.

Ye, J., Zheng, Y., Yan, A., Chen, N., Wang, Z., Huang, S., and Yang, Z. (2009). Arabidopsis formin3 directs the formation of actin cables and polarized growth in pollen tubes. Plant Cell 21: 3868–3884.

Yoro E, Nishida H, Ogawa-Ohnishi M, Yoshida C, Suzaki T, Matsubayashi Y, Kawaguchi M. (2019) PLENTY, a hydroxyproline O-arabinosyltransferase, negatively regulates root nodule symbiosis in Lotus japonicus. J Exp Bot. 70:507-517

Zhu X, Li S, Pan S, Xin X and Gua Y (2018) CSI1, PATROL1, and exocyst complex cooperate in delivery of cellulose synthase complexes to the plasma membrane. Proc Natl Acad Sci USA 115: E3578–E3587.

Figure legends

Fig. 1- Suppressor mutant frh1 increases the pollen fertility of hpat1 hpat3 plants

A) Both double mutant *hpat1/3* plants and the suppressed triple mutant *frh1 hpat1/3* plants appeared morphologically normal aside from differences in seed set. B) Average number of seeds per silique (±SD, N≥10 per genotype) for the indicated genotypes. The low seed set phenotype of *hpat1/3* double mutants is suppressed by *frh1*. High seed set is also observed for heterozygous *frh1* plants. Reciprocal crosses between *hpat1/3* and *frh1 hpat1/3* plants demonstrated that *frh1* suppression occurs in the pollen. '***' indicates a statistically significant difference (T-test P-value <0.0005) compared to the *hpat1/3* value for either the self-fertilized siliques or manually pollinated samples. NS is not significantly different. C) cleared siliques of WT Columbia, *hpat1 hpat3* and *frh1 hpat1/3* plants. WT and *frh1 hpat1/3* images are composite images to allow full silique imaging. D) Histogram of distribution of PT lengths after five hours of *in vitro* growth for the indicated genotypes. Data for all genotypes are statistically significantly different from both other genotypes (T-test P-value <0.005). E) *In vitro* grown PTs of the indicated genotypes. Scale bar = 100 μm.

Fig. 2- frh1 partially suppresses the disrupted polarity of cell wall polymers in hpat1/3 pollen tubes.

A) Wild-type Columbia-0 PT stained with JIM20 primary antibody and anti-rat FITC-conjugated secondary antibody. B) Left: Maximum projections of PTs stained with aniline blue fluorochrome (ABF). Right: quantification of signal intensity from the tip (distance on x-axis = 0) to 50 μm down the shaft of the PT (see Materials and Methods for more details concerning image analysis). Colored lines represent the mean fluorescent intensities for each genotype, and shading represents standard error. N ≥ 30 for each genotype. Vertical dashed line represents the approximate region of the PT where the apical dome transitions to the shaft. C) Left: Medial Z-slices of PTs stained with LM20 primary antibody and anti-rat FITC-conjugated secondary antibody. Right: quantification of fluorescence intensity as in B except measurements were taken to 25 μm from the tip. D) Left: Medial Z-slice of PTs stained with LM19 primary antibody and anti-rat FITC-conjugated secondary antibody. Right: quantification of signal intensity as in C. All images were acquired by confocal microscopy at 100x magnification and all scale bars = 10 μm.

Fig. 3- EXO70A2 is required for efficient pollen germination and pollen tube growth

A) Diagram of the *EXO70A2* coding sequence with the position of the *exo70a2-2* (G319E) missense mutation and insertion mutants *exo70a2-D* (Hála et al., 2008) and *exo70a2-3* marked. B) Semi-quantitative RT-PCR of flower cDNA samples from the indicated genotypes showing absence of transcript in the *exo70a2-3* plants using the primer pairs indicated in A. C) Average number of seeds per silique (±SD) for plants of the indicated genotype. Note the modest reduction in seed set for *exo70a2-3* in the wild-type background along with partial suppression of the *hpat1 hpat3* phenotype by this mutation. '***' mark statistically significant differences with the corresponding background (Columbia or *hpat1 hpat3*, T-test P-value <0.0005, N≥12). D) Cleared siliques of the *exo70a2* mutant alleles in the Columbia background, see Fig. 1D for Col comparison image. E and F) *in vitro* pollen germination samples of Columbia (E) and *exo70a2-3* (F) three hours after transfer to growth media. Inset in F shows non-

germinated *exo70a2-3* pollen grains. G) Quantification of pollen germination frequencies for WT, *exo70a2-2* and *exo70a2-3*. Mean of three replicates of ≥740 pollen grains, +/- SD. '**' marks significant difference between WT (T-test P-value <0.005). H-J) Alexander viability staining of anthers of WT (H), *exo70a2-2* (I) and *exo70a2-3* (J). Insets show free pollen grains. Note no difference in viability staining between genotypes. K and L) Pollen grains stained with Ruthenium red to mark pectin accumulation at the germination plaque. M) Histogram of PT lengths after five hours of *in vitro* growth for the indicated genotypes. Data for all genotypes are statistically significantly different from both other genotypes (T-test P-value <0.005, N≥200 per genotype). N) sustained growth rate of PTs of the indicated genotype. Mean, N≥21 tubes, ±SD. O and P) Differential interference contrast (DIC) micrograph of PTs.

Fig. 4- EXO70A2 localizes to the tip of growing pollen tubes

Representative PT expressing *EXO70A2:mNG* under its native promoter and co-stained with FM4-64 to visualize the plasma membrane. Single channels and merged image shown; overlapping signal is false-colored white. Imaged with confocal microscopy at 100x magnification. Scale bar represents 10 μm.

Fig. 5- Secretion of GF(EXT3)P is decreased in hpat1/3 exo70a2-2 pollen tubes

A) Schematic of the GF(EXT3)P construct, which includes the EXT3 signal peptide (SP), amino acids 1-175 of GFP, an 8x HIS tag, a portion of EXT3, a Myc tag, and amino acids 176-241 of GFP. B) Western blots (left) and corresponding Ponceau-stained membrane (right) of PT protein samples. * marks samples from plants carrying the *LAT52:GF(EXT3)P* transgene, NT is non-transgenic. An anti-GFP polyclonal antibody detects the fusion protein in the transgenic lines at the expected mass (~34 KDa). The reporter is also detected by the Hyp-Ara monocolonal antibody JIM20 only in the transgenic Col sample. C) Images of plasmolyzed PTs expressing *LAT52:GF(EXT3)P* (left) and non-transgenic control (right). Scale bar represents 10 μm. Arrows indicate the location of the PT cell wall tip, and arrowheads mark the plasma membrane. D) Quantification of secreted GFP signal reported as a secretion index (SI-see Materials and Methods for details, SI mean ± SE, N ≥ 30 PTs per genotype).

Samples labeled with the same letter are not significantly different (Benjamini–Hochberg FDR ≤ 0.05).

Fig. 6- Mutations in exocyst complex member sec15a also suppress the hpat1/3 fertility phenotype

A. Gene model diagram showing the relative position of insertion in the *sec15a-2* allele and the suppressor allele identified in *frh2* (*sec15a-3*). B) Segregation of the *sec15a-3* mutation in the *frh2 hpat1/3* BC5 F2 population. As expected for an *hpat1 hpat3* suppressing mutation, the number of homozygous wild-type *SEC15A* plants identified (+/+) was significantly below the expected value based on Mendelian segregation (chi-squared p-value =1.57 x 10^{-5}. C) Sample *sec15a-3* genotyping data for 15 *frh2 hpat1/3* BC5 F2 individuals visualized on an agarose gel. The wild-type allele is cleaved by digestion with MnlI. The single homozygous wild-type individual marked by '*' did not have the suppressive phenotype. D) Average number of seeds per silique (±SD) for plants of the indicated genotypes. *sec15a-2* is not transmitted through the male and not recoverable as a homozygous mutant (Hála et al., 2008). Both *sec15a* alleles suppress the *hpat1/3* phenotype with homozygous mutants showing stronger suppression than heterozygotes. 'ns' marks samples which were not statistically different from their corresponding background genotype. '***' marks statistically different samples (T-test P-value <0.0005, N≥11). E) Histogram of PT lengths after five hours of *in vitro* growth for the indicated genotypes. Data for all genotypes are statistically significantly different from both other genotypes (T-test P-value <0.005, N≥100 per genotype). F) Cleared siliques of the indicated genotypes. G) Average number of seeds per silique (±SD) for the indicated genotypes. All *hpat1/3*-based genotypes were siblings segregating from the same F2 population. '***' marks statistically different samples (T-test P-value <0.0005), '*' marks statistically significant samples T-test P-value <0.05, N≥15).

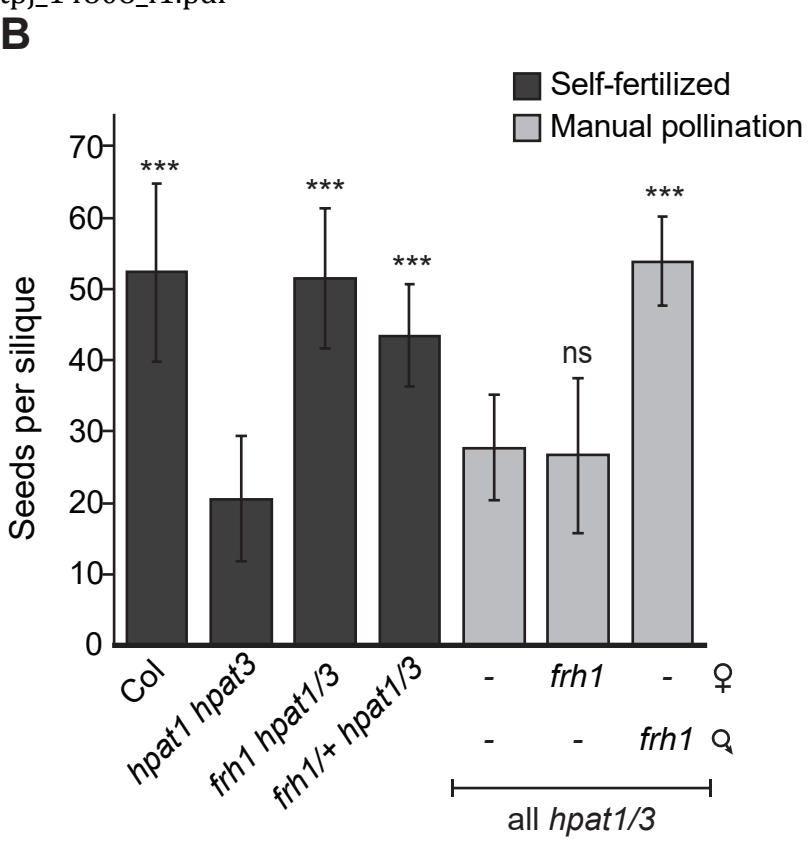

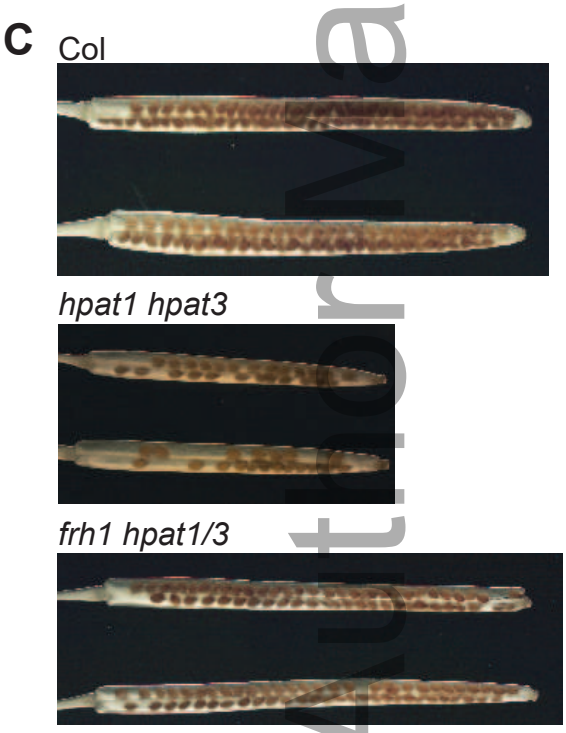

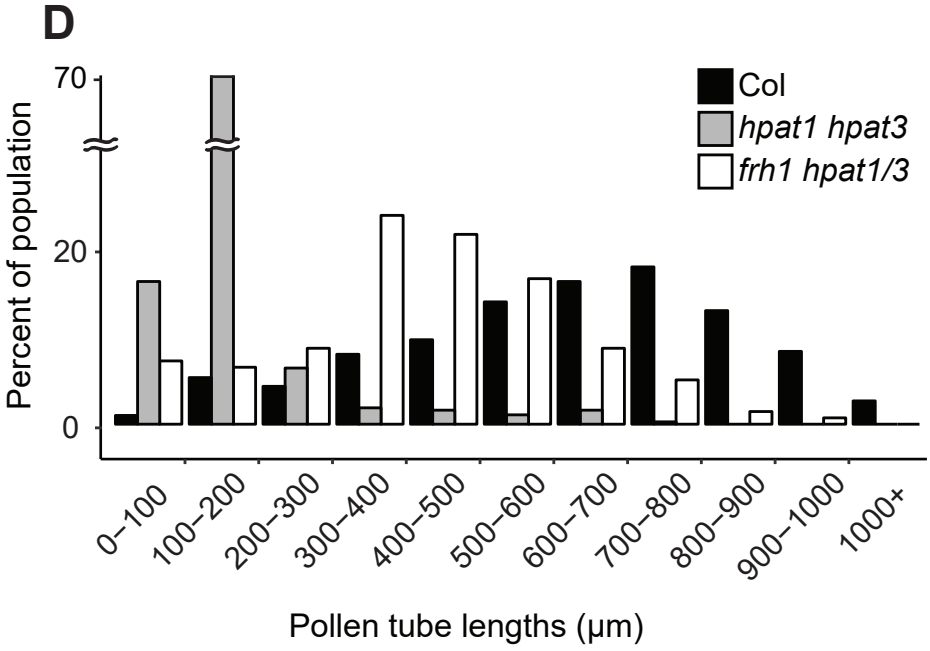

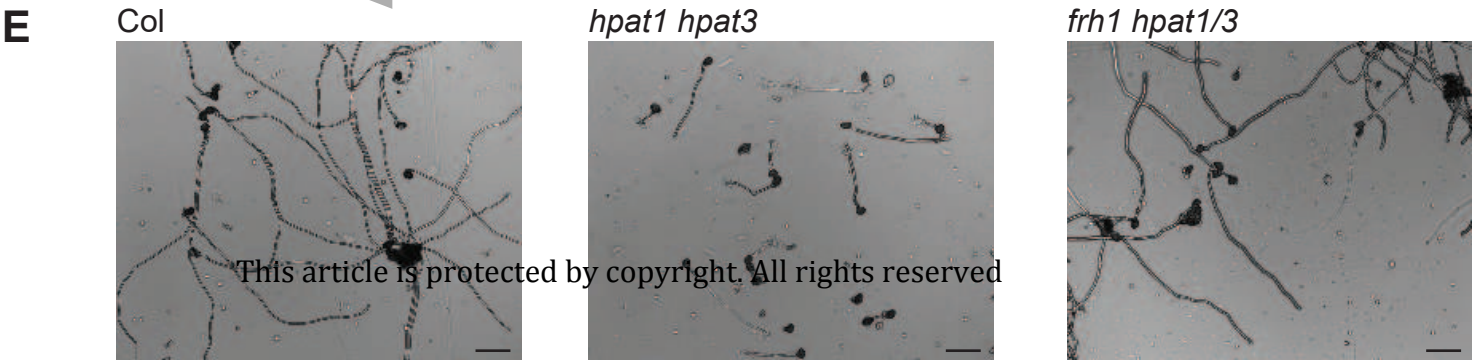

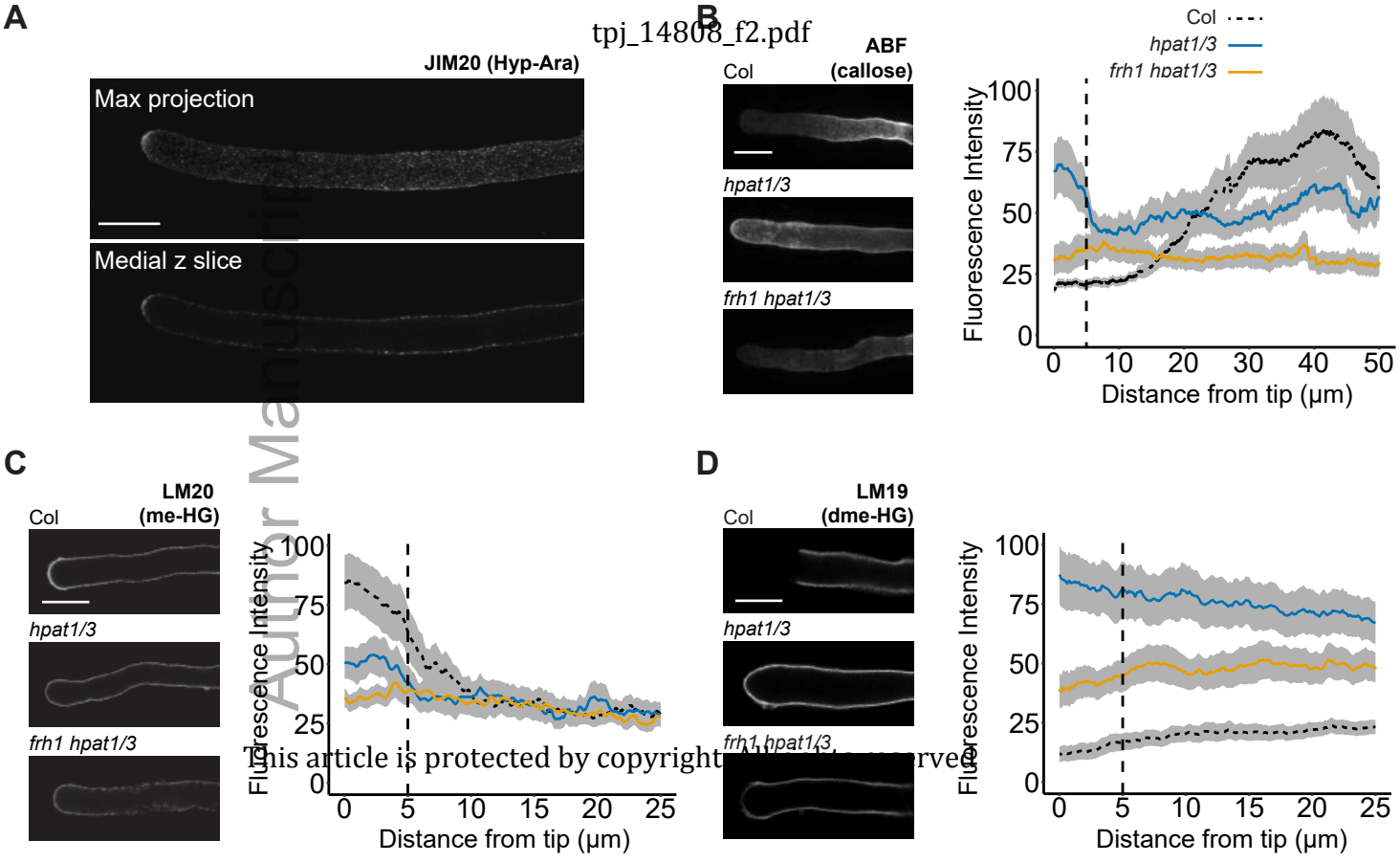

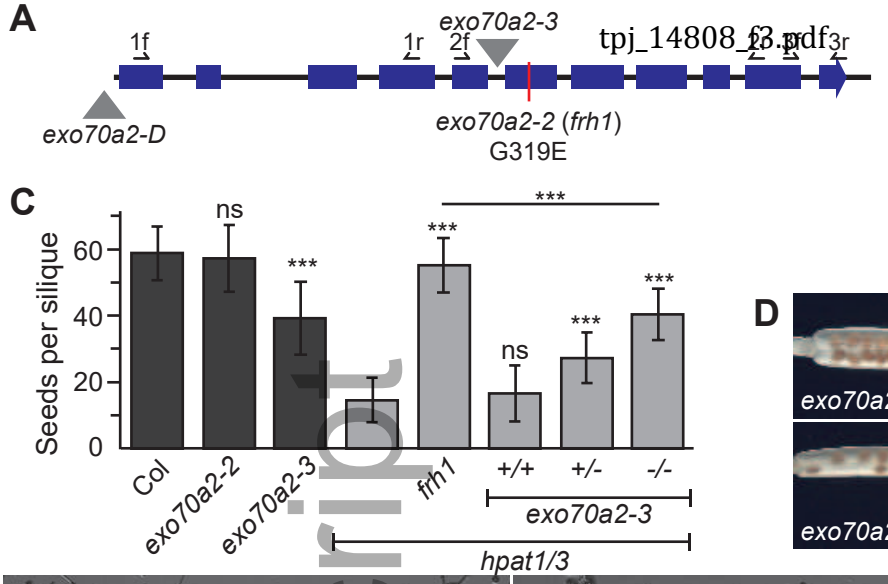

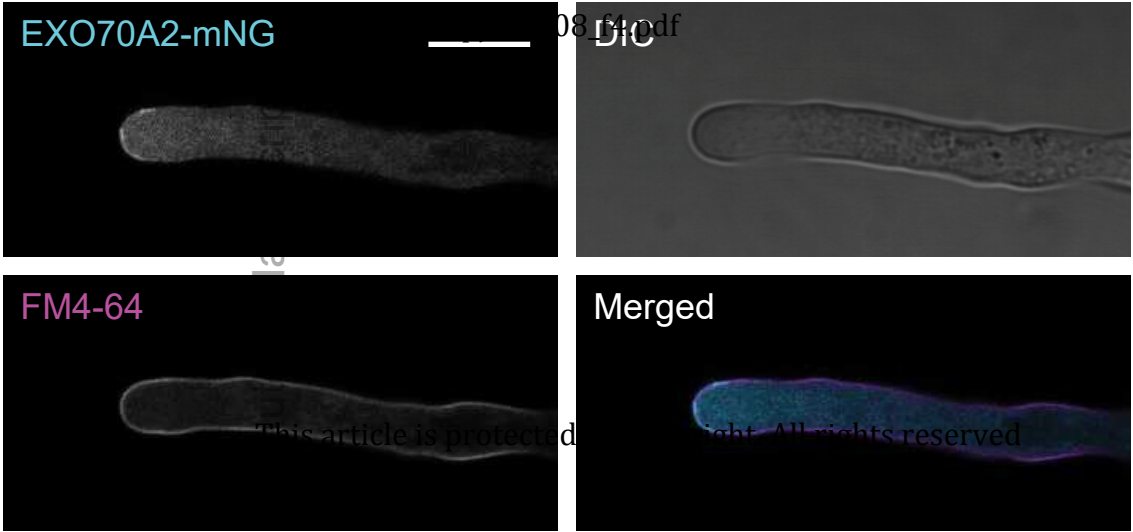

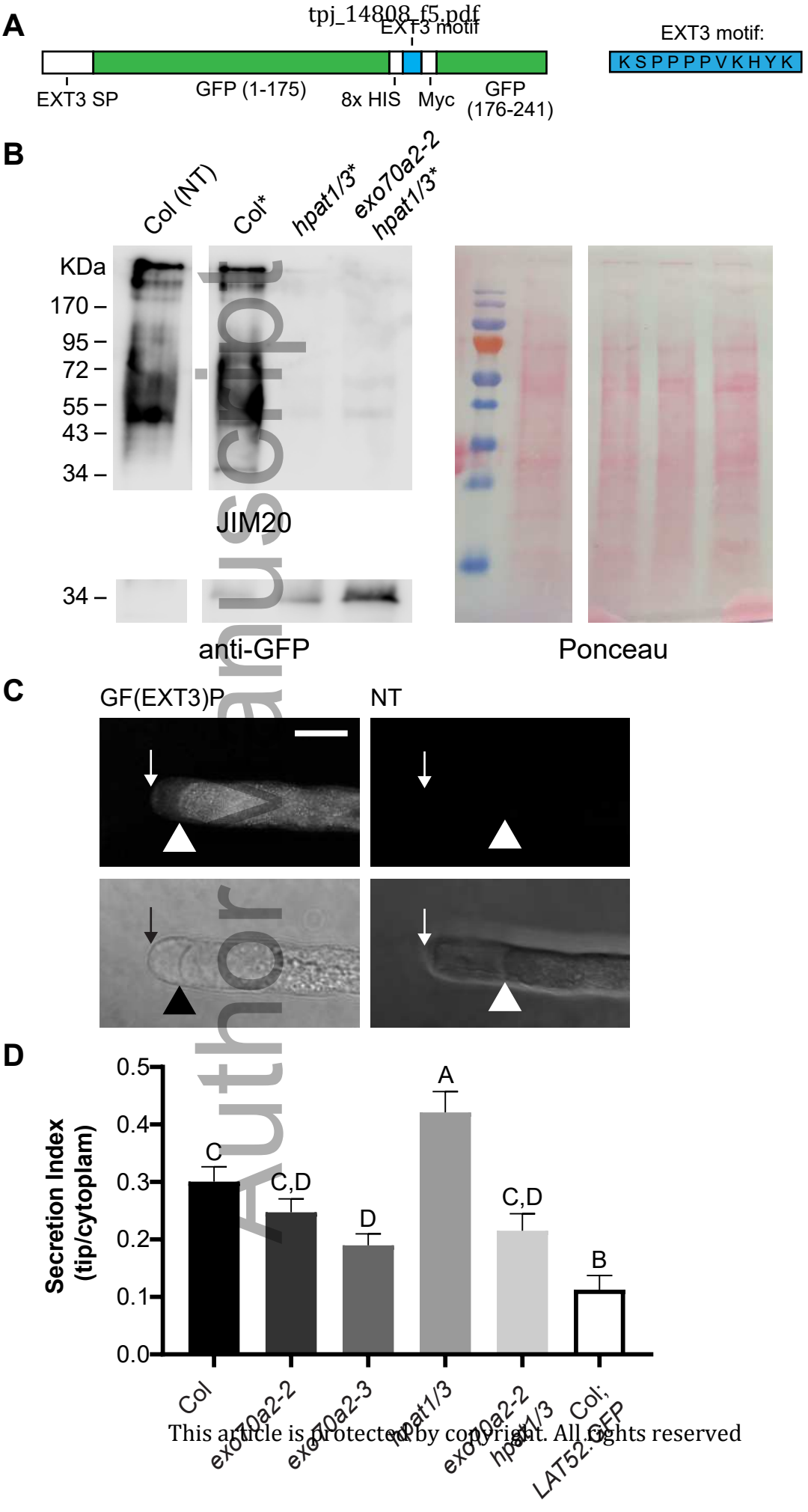

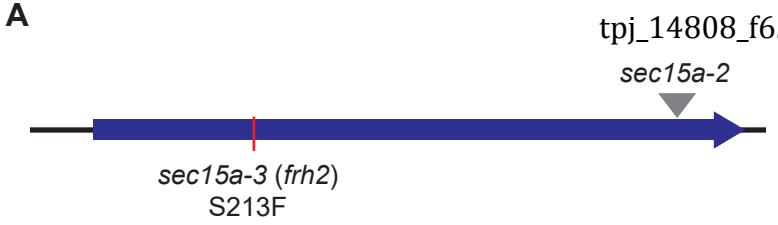

B

frh2 BC5 F2 segregation

sec15a2-3	N	%
+/+	1	2%
+/-	23	48%
-/-	24	50%
total	48